

50  
NATIONAL AERONAUTICS AND SPACE ADMINISTRATION

*Technical Report 32-1076*

*Radial Static Pressure Distributions in Confined  
Compressible Vortex Flow Fields*

*Thomas J. Pivrotto*

FACILITY FORM 602

N67-18655	
(ACCESSION NUMBER)	(THRU)
30	
(PAGES)	(CODE)
CR 82155	12
(NASA CR OR TMX OR AD NUMBER)	(CATEGORY)

JET PROPULSION LABORATORY  
CALIFORNIA INSTITUTE OF TECHNOLOGY  
PASADENA, CALIFORNIA

March 1, 1967

NATIONAL AERONAUTICS AND SPACE ADMINISTRATION

*Technical Report 32-1076*

*Radial Static Pressure Distributions in Confined  
Compressible Vortex Flow Fields*

*Thomas J. Pivrotto*

Approved by:

A handwritten signature in dark ink, appearing to read 'D. R. Bartz', is written over a horizontal line.

D. R. Bartz, Manager  
Research and Advanced Concepts Section

JET PROPULSION LABORATORY  
CALIFORNIA INSTITUTE OF TECHNOLOGY  
PASADENA, CALIFORNIA

March 1, 1967

Technical Report 32-1076

Copyright © 1967  
Jet Propulsion Laboratory  
California Institute of Technology  
Prepared Under Contract No. NAS 7-100  
National Aeronautics & Space Administration

## Contents

<b>I. Introduction</b>	1
<b>II. Experimental Equipment and Techniques</b>	2
A. Vortex Tube	2
B. Pressure and Temperature Measurements	2
<b>III. Results</b>	3
<b>IV. Discussion</b>	23
<b>V. Conclusions</b>	24
<b>Nomenclature</b>	25
<b>References</b>	25

### Table

1. Computed values of the effective radial Reynolds number and core radius	13
--	----

### Figures

1. Schematic diagram of gaseous-vortex separator	2
2. Experimental vortex tube	3
3. Radial static pressure distributions, 0.25-in. exit hole diameter	4
4. Radial static pressure distributions, 0.63-in. exit hole diameter	5
5. Radial static pressure distribution, 2.50-in. exit hole diameter	6
6. Radial Mach number and velocity distribution, 0.63-in. exit hole diameter, low mass flow rate	7
7. Radial Mach number and velocity distribution, 0.63-in. exit hole diameter, high mass flow rate	8
8. Radial Mach number and velocity distribution, 2.50-in. exit hole diameter	9
9. Effect of exit hole diameter and mass flow rate on the maximum tangential Mach number	15
10. Effect of exit hole diameter and mass flow rate on ratio of the maximum to the peripheral Mach number	16
11. Effect of exit hole diameter and mass flow rate on the radial location of the maximum tangential Mach number	17
12. Effect of exit hole diameter and mass flow rate on the peripheral tangential velocity	18
13. Velocity of the driving jets at the jet tube exit plane	19
14. Cylindrical wall static pressure	20
15. Vortex tube manifold pressure	21
16. Relationship between the peripheral tangential and radial velocities	21
17. Static pressure at center of closed end wall	22

## **Abstract**

A confined vortex flow was studied to determine the effect of the fluid mass flow rate and the exit orifice diameter on the radial static-pressure distribution for a given vortex tube diameter, length, and injection configuration. The exit hole diameter had a significant effect on the radial pressure distribution, and the mass flow rate lost its influence on the pressure distribution beyond a limiting value, which increased with increasing exit hole diameter. From 50 to 90% of the fluid momentum was lost at the cylindrical wall. A method was also developed for determining the effective radial Reynolds number and effective exit hole radius from the experimentally determined maximum tangential Mach number and its radial location.

# Radial Static Pressure Distributions in Confined Compressible Vortex Flow Fields

## I. Introduction

In order to take full advantage of the inherent potential of nuclear fuel as a direct source of energy for rocket propulsion, a means must be found to circumvent the constraints imposed on system performance by the temperature limitations of solid-fuel elements. A desirable scheme would be one in which a very-high-temperature, gaseous, fissioning fuel and a gaseous propellant are mixed together so that the energy can be transferred directly from fuel to propellant particles by collisions and radiation absorption. It would then be possible to attain propellant temperatures substantially higher than those that are achieved with solid-fuel elements. Because of biological, economic, and performance considerations it would then be essential, however, to separate most of the fuel gas from the hot propellant gas before the latter is expelled through a nozzle.

One such scheme, designated as a gaseous-vortex reactor, is presented and partially analyzed in Ref. 1 and is shown schematically in Fig. 1. The gaseous-vortex-reactor concept takes advantage of the strong radial pressure gradient generated by a vortex-type flow to induce radial diffusion between the low molecular weight propellant gas and the much higher molecular weight fuel gas. Theoretically, the results of this binary diffusion

phenomenon would be to separate and retain the fuel gas inside the reactor while the propellant flows through. The theoretical distribution of fuel gas inside the cylindrical vortex tube would produce a low concentration near the cylindrical wall and near the centerline and a high concentration within an annular region of small radial increment. Conceptually, the propellant gas, which is injected tangentially into the vortex tube at the cylindrical wall to sustain the rotational flow field, migrates radially inward through the dense, hot, annular cloud of fissioning fuel and then flows axially out through a hole in the center of one end wall.

Since the crux of the separation process of the gaseous-vortex-reactor concept is the radial pressure gradient, or more precisely the radial gradient of the log of static pressure  $d \ln p/dr$ , the radial distribution of static pressure has been investigated both experimentally and analytically. In this report, the results of an experimental program designed to measure the effect of the diameter of the orifice through which the fluid leaves the vortex tube and the effect of mass flow rate on the static pressure distribution are presented. Also, certain results of this experimental investigation are compared with several analytic descriptions of confined vortex flows found in the literature.

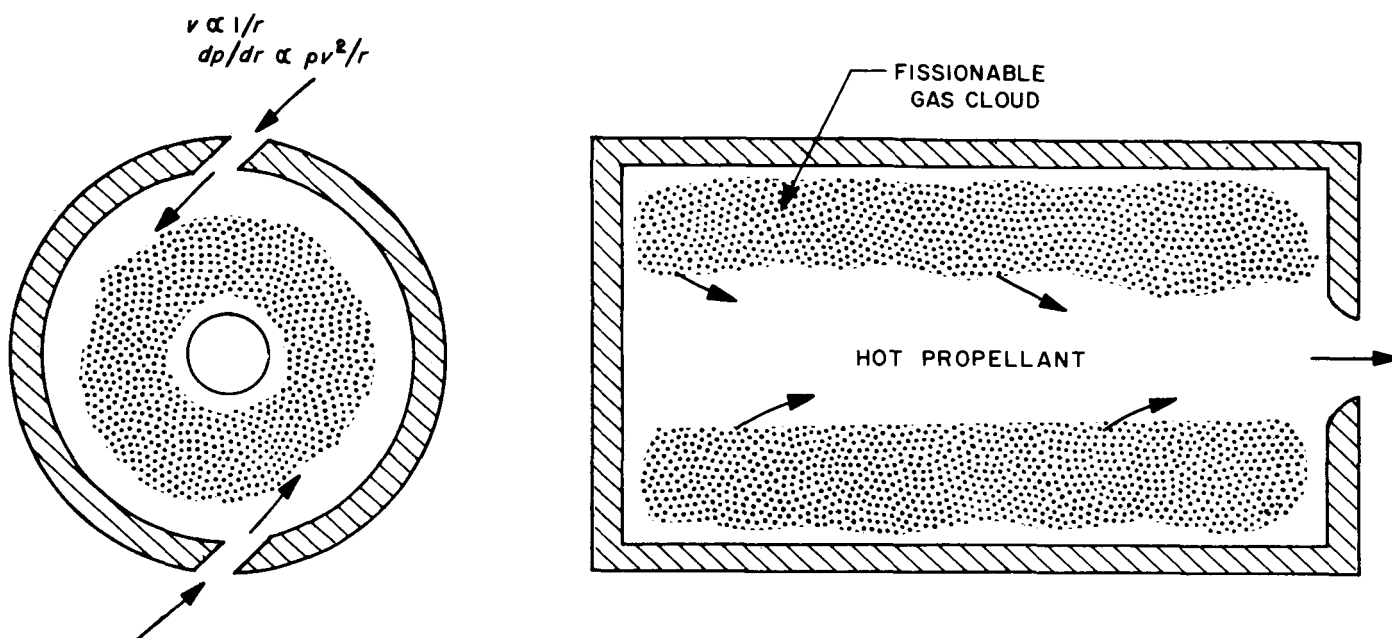


Fig. 1. Schematic diagram of gaseous-vortex separator

## II. Experimental Equipment and Techniques

### A. Vortex Tube

The vortex tube used for this investigation was a right circular cylinder with an internal diameter of 4.50 in. and an internal length of 24.14 in. The exit orifice, a simple cylindrical hole located at the center of one end wall, was varied from 0.25 to 2.50 in. in diameter in 12 steps, as one test parameter. Nitrogen was used as the working fluid and the mass flow rate was varied between 0.012 and 0.204 lbm/sec, as the second parameter. However, it was not possible to vary the flow rate over the full range for any one exit orifice diameter because of pressure limitations on the apparatus.

A drawing of the vortex tube is shown in Fig. 2. This apparatus consisted of two concentric steel tubes held together at both ends by flanges onto which the end walls were bolted. The annular space between the tubes served as a manifold which supplied the high-pressure gas to each of 804 jet tubes. These jet tubes were fabricated of 0.062-in. outside diameter by 0.007-in. inside diameter stainless steel tubing cut into 0.90-in. lengths and cemented into holes drilled through the wall of the inner tube. The overall effect of this arrangement was to have 0.007-in.-diameter driving jets arranged in a helix and tangent to a circle whose diameter was 92% of the inner tube's inside diameter. The helix contained

six jets per cycle and had a pitch of 0.180 in.; this pattern of jets covered the entire inner cylindrical surface of the vortex tube. For all experiments the fluid, nitrogen, was discharged into the atmosphere through the exit hole in the end wall.

### B. Pressure and Temperature Measurements

A pitot tube and a bare-wire thermocouple were used to measure the fluid stagnation pressure and temperature 15 in. upstream of a choked venturi located in the line that supplied the high-pressure nitrogen to the vortex tube manifold. From these pressure and temperature data and the known characteristics of the venturi, the nitrogen mass flow rate was determined. The manifold pressure and temperature were similarly measured for each experiment. In addition, the static pressure at the vortex tube cylindrical wall, measured at the closed end of the tube, was monitored and held constant during each run.

The radial static-pressure distribution on the closed end wall of the vortex tube was measured with a pressure tap located in a disk that was built into the end wall and could be rotated, as shown in Fig. 2. The pressure tap had a diameter of 0.010 in. and was approximately 0.020 in. deep. This disk had its axis displaced 1.062 in. from the vortex tube centerline and was flush with the inner surface of the end wall. By rotating the disk, the

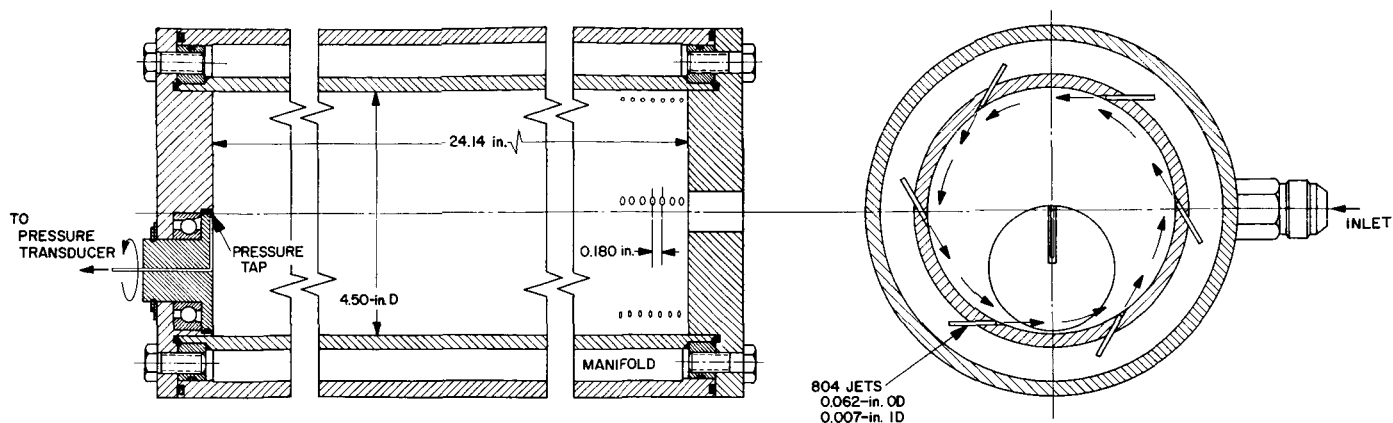


Fig. 2. Experimental vortex tube

static pressure could be determined at any radial position from the centerline to a point 0.127 in. from the cylindrical surface of the vortex tube.

The radial position of the pressure tap was determined by gearing a selsyn motor to the disk. The radial position of the pressure tap in the vortex tube,  $r$ , was equal to the chord distance between the vortex tube centerline and the tap position near the disk periphery, or  $r = 2a \times \sin \theta/2$ . The constant  $a$ , equal to 1.062 in., was the fixed distance between the disk center and the pressure tap location, and  $\theta$  was the disk's angular rotation measured from the vortex tube centerline. (Since the selsyn output is proportional to  $\sin \phi$ , where  $\phi$  is the angular rotation of the selsyn shaft,  $r$  is directly proportional to the selsyn output if a 2-to-1 gear ratio between selsyn and disk is used, so that  $\phi = \theta/2$ .) A rectified signal from the selsyn motor could then be fed directly to the  $x$ -axis of an  $x$ - $y$  plotter. A pressure transducer was connected to the pressure tap through a short piece of tubing and its signal fed to the  $y$ -axis of the plotter. In this way, a trace of  $p = p(r)$  was automatically obtained by rotating the disk through 180 deg. This procedure was repeated for each exit hole diameter and for several mass flow rates at each diameter.

To prevent galling, some clearance had to be provided in the form of an annular gap between the disk and the end wall. It was expected that fluid would be trapped in the annular gap and driven radially inward by the radial pressure gradient. This fluid would erupt from the gap near the vortex tube centerline and disturb the end wall boundary layer. To minimize this effect, the disk was carefully fitted into a 0.0003-in. radially oversized hole machined in the end wall. The fluid was pre-

vented from leaking out through this gap by an O-ring located 0.050 in. beneath the inner surface of the end wall. Therefore, the resulting gap was approximately 0.0003 in. wide and 0.050 in. deep.

### III. Results

The radial static-pressure distributions obtained with the minimum exit hole diameter (0.25 in.), with one intermediate diameter (0.63 in.), and with the maximum diameter (2.50 in.) are shown in Figs. 3, 4, and 5 respectively. The cylindrical wall static pressure  $p_w$  is the parameter in Figs. 3 and 4 and varies from approximately 100 to 500 cm Hg (abs). With the maximum exit hole diameter, Fig. 5, the maximum wall pressure possible was 100 cm Hg (abs) because of pressure limitations on the vortex tube manifold and the supply system. For convenience, the scales on the  $x$ - $y$  plotter were adjusted for each experiment so that the maximum pressure sensed by the probe was plotted as 1.0 at a radius of 1.0. This maximum sensed pressure  $p_p$  was the pressure at a radius of 2.12 in., since that was the furthest point to which the pressure tap could be moved. Therefore, the recorded data, examples of which are reproduced in Figs. 3, 4, and 5, are distributions of the pressure ratio  $p/p_p$  with respect to the radius ratio  $r/r_p$ , where  $r_p = 2.12$  in. Hence the radius  $r_p$  defines a cylindrical surface that bounds the vortex flow field within which the detailed pressure distributions were made. The absolute value of the pressure  $p_p$  was determined by making a linear extrapolation out to the cylindrical wall of the vortex tube,  $r_w = 2.250$  in., and using the independently measured wall pressure  $p_w$ . For most experiments, the difference between  $p_p$  and  $p_w$  was found to be less than the experimental uncertainty, and the maximum difference was found to be 2% of  $p_w$ .



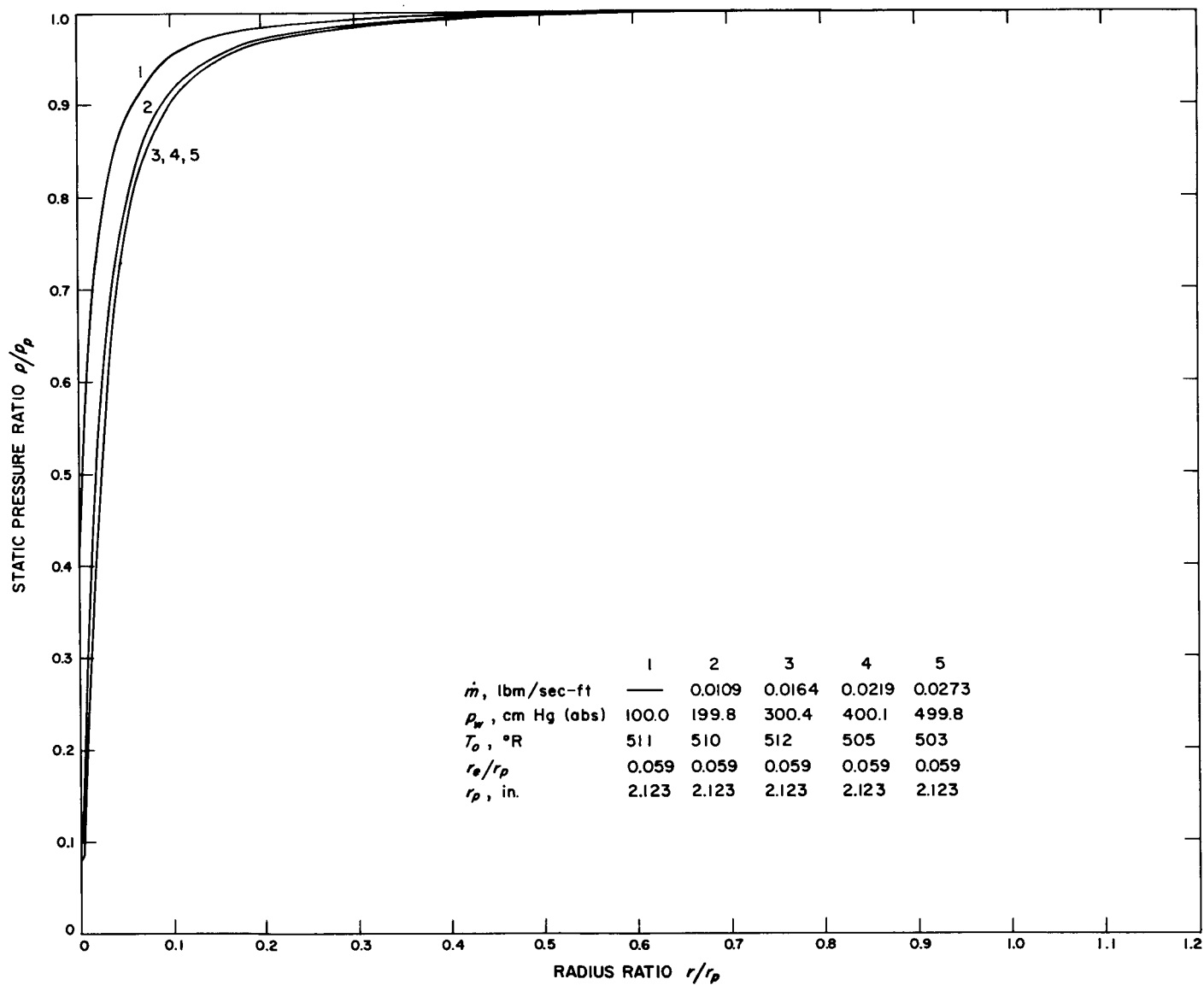


Fig. 3. Radial static pressure distributions, 0.25-in. exit hole diameter

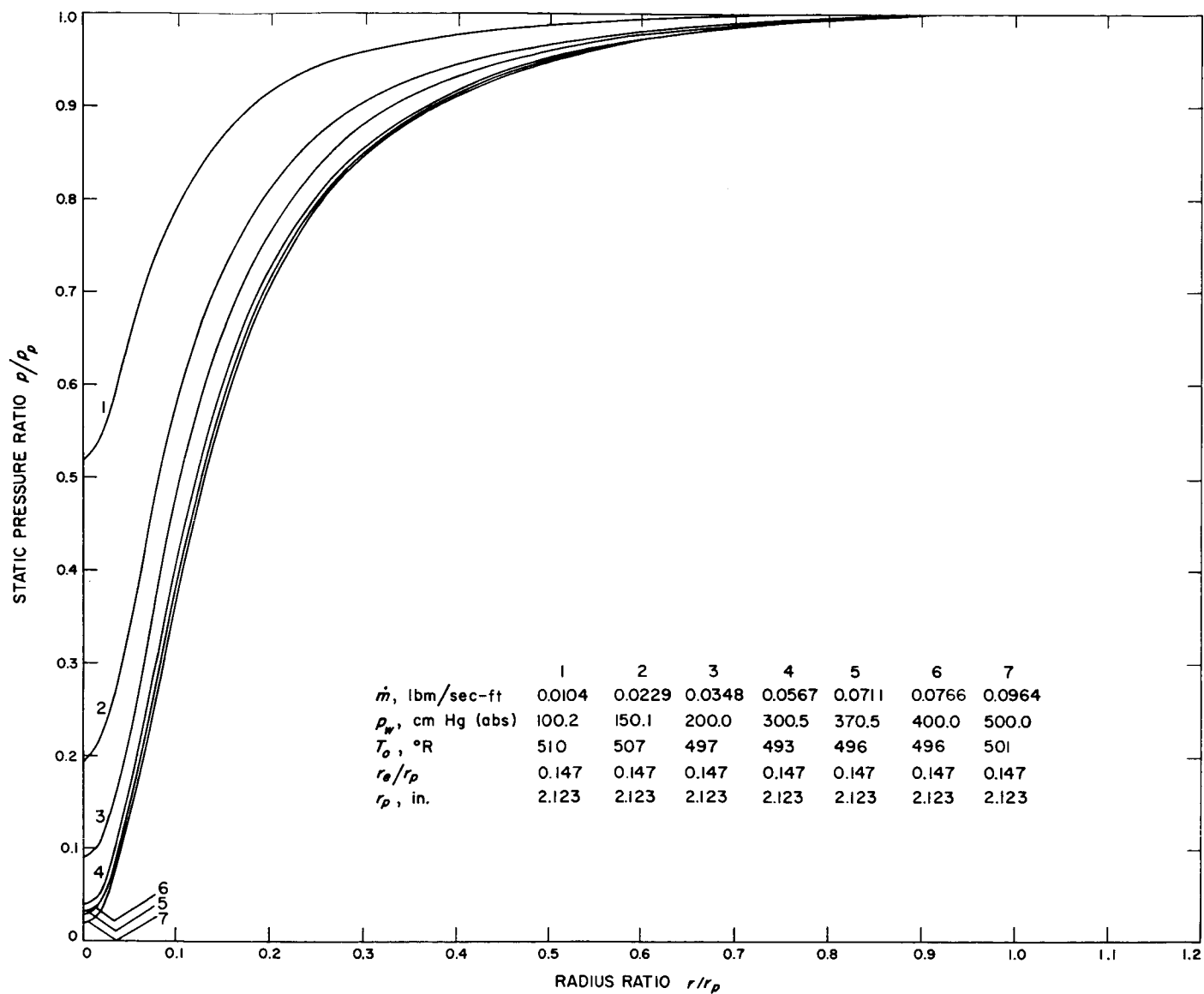


Fig. 4. Radial static pressure distributions, 0.63-in. exit hole diameter

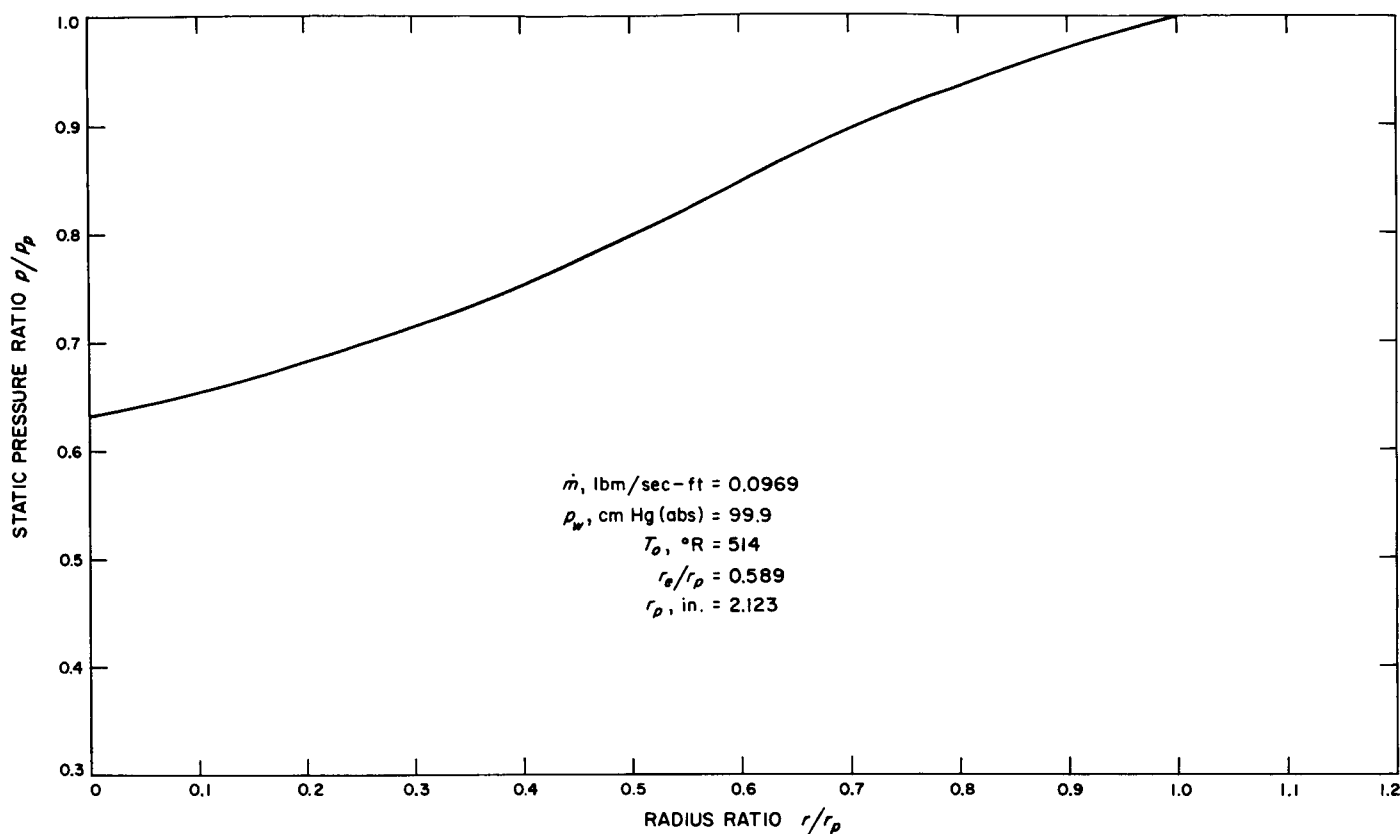


Fig. 5. Radial static pressure distribution, 2.50-in. exit hole diameter

The tangential Mach number  $M$  can be computed from the pressure distributions by using the radial momentum equation when this equation is simplified by assuming that the radial and axial velocities and all tangential gradients and body forces are zero and that the flow is steady in time. The resulting equation, which expresses the fact that the change of linear momentum of each fluid particle is exactly balanced by the local radial pressure gradient, is

$$M^2 = \frac{\frac{r}{r_p} \frac{d p}{p_p}}{\gamma \frac{p}{p_p} \frac{d r}{r_p}} \quad (1)$$

To compute the tangential Mach number from pressure distributions as shown in Figs. 3, 4, and 5, the pressure gradient

$$\frac{d \frac{p}{p_p}}{d \frac{r}{r_p}}$$

was determined graphically from the distributions. Equation (1) was applied to the two pressure distributions in Fig. 4 corresponding with the minimum and maximum wall pressure  $p_w$  for the 0.63-in.-diameter exit hole and to the pressure distribution of Fig. 5 where the exit hole diameter was 2.50 in. The resulting radial distributions of the tangential Mach number are shown in Figs. 6, 7, and 8, where the Mach number has been normalized with respect to the tangential Mach number at the reference radius  $r_p$ .

Also shown in Figs. 6, 7, and 8 are radial distributions of the tangential velocity ratio  $v/v_p$  computed from the solution of a particular form of the tangential momentum equation to be discussed subsequently. When comparing Mach number distributions with the corresponding velocity distributions, as is done in Figs. 6, 7, and 8, the assumption of an isothermal flow is implied. The radial static-temperature distribution, inferred from bare-wire thermocouple data, has been obtained in a similar vortex flow field and published in Ref. 2. It was found that the static temperature varied monotonically from 528°R at the periphery to 450°R at a point very close to the centerline. The temperature then was assumed to increase to

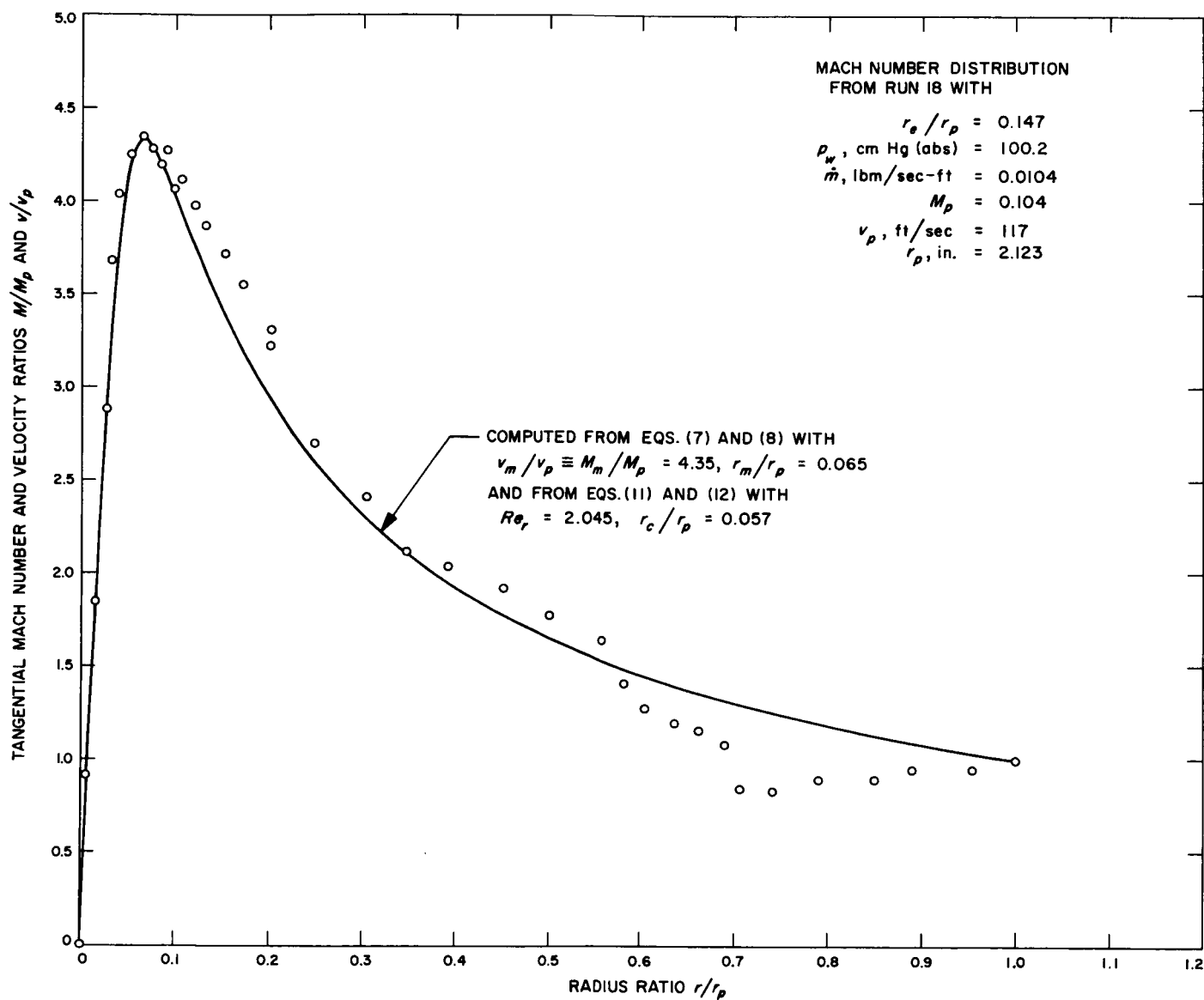


Fig. 6. Radial Mach number and velocity distribution, 0.63-in. exit hole diameter, low mass flow rate

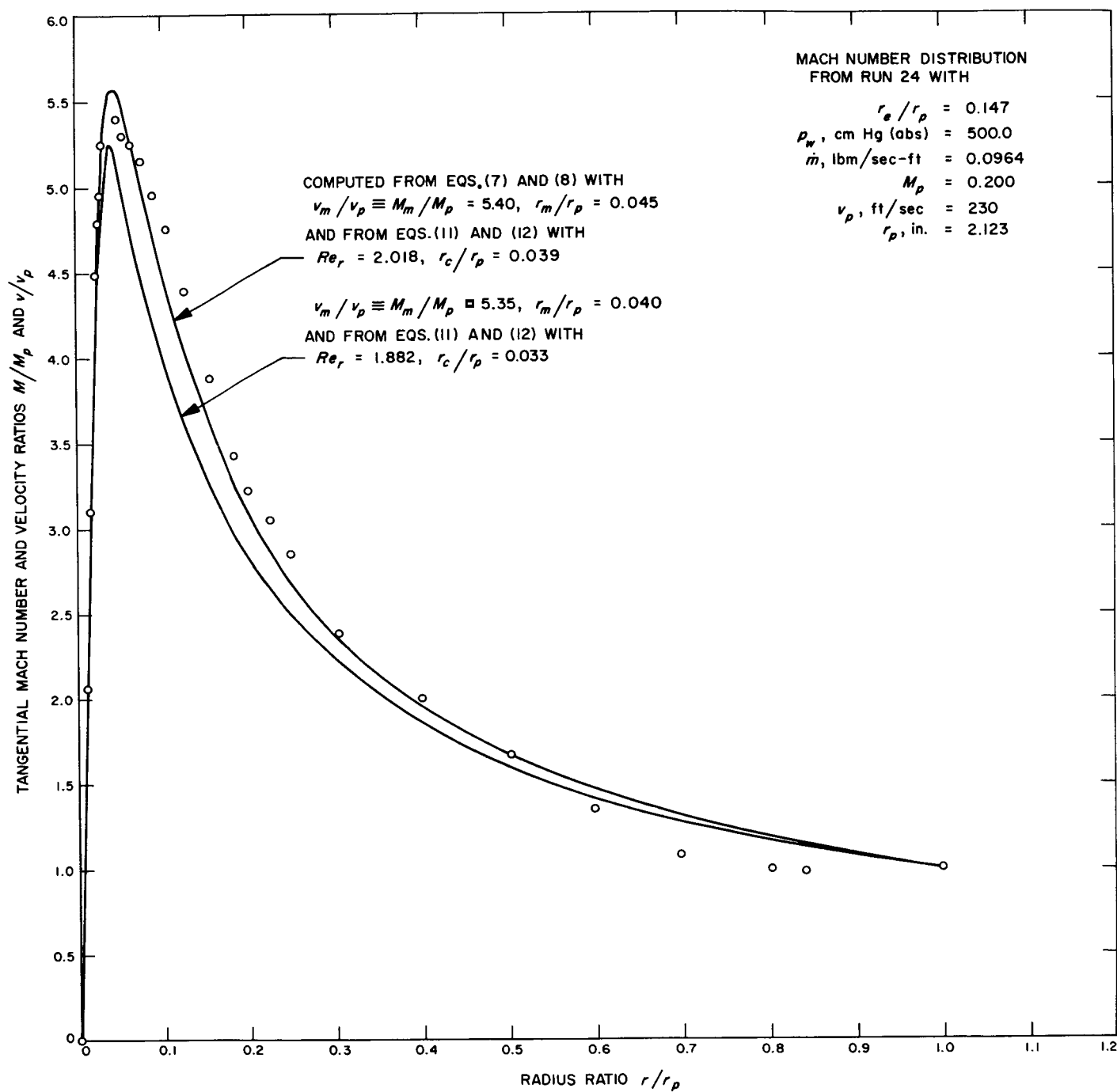


Fig. 7. Radial Mach number and velocity distribution, 0.63-in. exit hole diameter, high mass flow rate

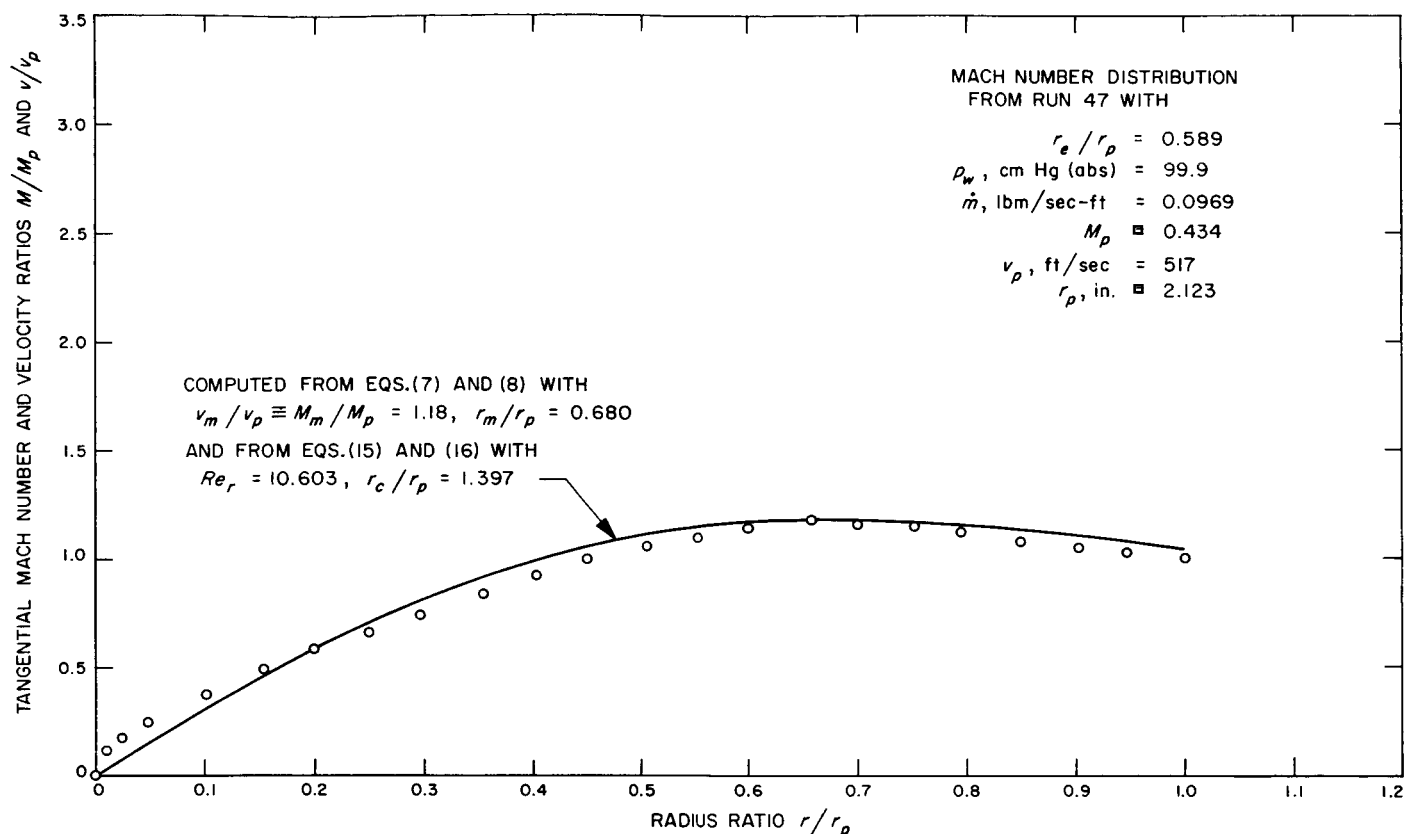


Fig. 8. Radial Mach number and velocity distribution, 2.50-in. exit hole diameter

507°R at the centerline, where all velocity components were taken to be zero. This temperature variation would cause the Mach number to be, at most, approximately 8% greater than the corresponding velocity. Hence, com-

paring Mach number and velocity distributions directly is reasonable, since the determination of Mach number from the pressure profiles and of velocity from an assumed analytical model are themselves subject to some error.

The form of the tangential momentum equation used to predict the radial distribution of tangential velocity shown in Figs. 6, 7, and 8 was obtained by first assuming the flow to be steady in time and axisymmetric, with no body forces acting and with a constant coefficient of viscosity. Applying these assumptions (which, with the possible exception of the last, are believed to be reasonable) to the general tangential momentum equation, found in Ref. 3 for cylindrical coordinates, the following equation is obtained:

$$u \frac{\partial v}{\partial r} + w \frac{\partial v}{\partial z} + \frac{uv}{r} = \nu \left( \frac{\partial^2 v}{\partial r^2} + \frac{1}{r} \frac{\partial v}{\partial r} - \frac{v}{r^2} + \frac{\partial^2 v}{\partial z^2} \right) \quad (2)$$

This equation has been discussed extensively in Refs. 4 through 8. If the second term on the left and the last term on the right are dropped, that is, if  $v$  is assumed to be independent of  $z$ , and if a suitable assumption is made for the radial distribution of  $ur/\nu$ , the equation becomes tractable.

Although it has been shown in Refs. 7 and 8 that in the flows of interest,  $(\partial\Gamma/\Gamma w)/(\partial z/l)$  is small, the question of omitting those terms involving  $\partial v/\partial z$  in Eq. (2) must take into consideration the relative magnitude of the various other

terms. To this end, an order-of-magnitude analysis of Eq. (2) was made. The tangential velocity was assumed to be given by  $v = cr^n$  and the various terms of Eq. (2) were evaluated to obtain the following results:

$$n + \frac{w}{uv} \frac{\partial vr}{\partial z} + 1 = \frac{v}{ur} \left( n(n-1) + n - 1 + \frac{r}{v} \frac{\partial^2 vr}{\partial z^2} \right) \quad (3)$$

It has been shown by experiment (Ref. 9) that at large radii, where the tangential velocity is inversely proportioned to the radius,  $n$  is approximately  $-0.7$ . Also, from inspection of experimentally determined tangential Mach number distributions, it can be seen that  $n$  must become approximately 1 for small radii. Therefore, over most of the flow field, the radial terms in Eq. (2) are of order 1 and the remaining terms can be dropped only if they are of order less than 1. The part of the term on the left,  $(1/uv) (\partial vr/\partial z)$ , was evaluated by using the results of Ref. 7 and assuming that the radial velocity was constant and equal to the value  $u_w$  computed from the measured  $\dot{m}$ ,  $p_w$ , and  $T_o$ . This last assumption implies that the mass flow rate is a linear function of radius, or

$$\dot{m} = \dot{m}_w \frac{r}{r_w} \quad (4)$$

and is in approximate agreement with the results of Ref. 8. Note that the mass flow rate difference  $[\dot{m}_w - \dot{m}(r)]$  is that mass flow absorbed by the end wall boundary layers. It was found that  $(1/uv) (\partial vr/\partial z)$  in Eq. (3) varied between approximately  $10^{-2}$  and  $10^{-3}$  for the experiments of this investigation. Hence, provided the axial velocity  $w$  was of the order of 10 to 100 ft/sec or less, depending on the experiment, this axial term was relatively small. The axial term on the right side of Eq. (3) was evaluated by assuming that the gradient  $\partial vr/\partial z$  varied linearly with  $z$ ; it was found that this term was at most of order  $10^{-5}$  and hence insignificant. Therefore, providing the axial velocity is small, the following form of the tangential momentum equation, which was used in Refs. 4-8, applies here:

$$\frac{1}{r} \frac{dv}{dr} + \frac{v}{r^2} = \frac{v}{ur} \left( \frac{d^2 v}{dr^2} + \frac{1}{r} \frac{dv}{dr} - \frac{v}{r^2} \right) \quad (5)$$

In the core of the flow,  $n$  is approximately equal to 1, so that the first term on the right of Eq. (3) also becomes relatively very small and therefore can also be neglected.

Equation (5) can readily be solved if the parameter  $ur/v$  is either constant or proportional to the radius  $r$  or to  $r^2$ . As has been done before, the vortex flow field was divided into a central core, in which  $ur/v$  was allowed to vary with  $r^2$ , and an outer annular region, in which  $ur/v$  was assumed constant. The radius dividing these two regions will be denoted by  $r_c$ . For an incompressible, constant-viscosity fluid, the steady-state axisymmetric continuity equation is

$$\frac{1}{r} \frac{\partial ur}{\partial r} + \frac{\partial w}{\partial z} = 0 \quad (6)$$

This equation shows that the assumptions above on the distribution of  $ur/v$  lead to an axial velocity  $w$  that is linearly proportional to the axial coordinate  $z$  in the core ( $r < r_c$ ) and is independent of  $z$  for  $r > r_c$ .

It is convenient to write Eq. (5) in terms of  $vr$ . The boundary conditions then are  $vr = v_p r_p$  at  $r = r_p$  for the outer annulus and  $vr = 0$  at  $r = 0$  for the core. The second two necessary boundary conditions are obtained by matching the outer and inner solutions at  $r_c$ ; hence

$$(vr)_{\text{annulus}} = (vr)_{\text{core}}$$

and

$$\left(\frac{dvr}{dr}\right)_{\text{annulus}} = \left(\frac{dvr}{dr}\right)_{\text{core}}$$

at  $r = r_c$ . The solution of Eq. (5) is then

$$\frac{v}{v_p} = \frac{(2 - Re_r) \exp(\frac{1}{2} Re_r) \left\{ 1 - \exp \left[ - \left( \frac{r}{r_p} / \frac{r_c}{r_p} \right)^2 \frac{1}{2} Re_r \right] \right\} \left( \frac{r}{r_p} \right)^{-1}}{[(2 - Re_r) \exp(\frac{1}{2} Re_r) - 2] + Re_r \left( \frac{r_c}{r_p} \right)^{Re_r - 2}} \quad (7)$$

in the core and

$$\frac{v}{v_p} = \frac{[(2 - Re_r) \exp(\frac{1}{2} Re_r) - 2] \left( \frac{r}{r_p} \right)^{-1} + Re_r \left( \frac{r_c}{r_p} \right)^{Re_r - 2} \left( \frac{r}{r_p} \right)^{1 - Re_r}}{[(2 - Re_r) \exp(\frac{1}{2} Re_r) - 2] + Re_r \left( \frac{r_c}{r_p} \right)^{Re_r - 2}} \quad (8)$$

outside the core. Since the parameter  $ur/\nu$  is the ratio of the radial inertia force to the viscous force, it has been called the radial Reynolds number. Hence the substitution  $Re_r \equiv -ur/\nu$  was made. Both solutions, Eqs. (7) and (8), are indeterminate for  $Re_r = 2$ ; hence Eq. (5) must be solved separately for this particular value of  $Re_r$ . This has been done in Refs. 4, 5, and 6 and will not be repeated here, since one is not likely to achieve a precise value of 2 for  $Re_r$  in any given experiment.

To compute the complete radial distribution of the tangential velocity from Eqs. (7) and (8), as was done for Figs. 6, 7, and 8, values must be assigned to the parameters  $r_c$  and  $Re_r$ . Note that the parameter  $Re_r$  is equal to  $\dot{m}/2\pi\mu$  where  $\dot{m}$  is the mass flow rate per unit length of vortex tube. If  $Re_r$  is computed from the measured total mass flow rate for a given experiment and if  $r_c$  is taken as the radius of the exit hole, the resulting velocity distribution is found to be considerably different from that computed from the radial static pressure distribution (see, for example, Ref. 10). In order to get reasonable agreement between the analytic and experimental velocity distributions, a trial-and-error procedure was followed in Ref. 10 to find the "right" values for  $r_c$  and  $Re_r$ . For the particular set of conditions chosen in Ref. 10,  $r_c$  was found to be considerably less than the exit hole radius  $r_e$ , and  $Re_r$  was found to be considerably less than  $\dot{m}/2\pi\mu$ .

In order to determine the appropriate values of  $r_c$  and  $Re_r$  for each of the large number of experiments of this investigation, an alternate procedure has been developed. This procedure is based on the observation that the two most prominent characteristics of the radial Mach number distributions are the maximum Mach number and its radial position. From these two experimental quantities, the parameters  $r_c$  and  $Re_r$  were uniquely determined. By using these values of  $r_c$  and  $Re_r$  in Eqs. (7) and (8), the velocity distributions of Figs. 6, 7, and 8 were obtained. Notice that the computed velocity distributions do not pass through the reference points  $M_m/M_p$  in Figs. 6 and 7 or through  $M/M_p = 1$  at  $r/r_p = 1$  in Fig. 8. These anomalies are simply due to round-off errors incurred in the hand computations; however, they illustrate the sensitivity of the equations to small errors. For example, two sets of  $M_m/M_p$ ,  $r_m/r_p$  were assumed for the experimental distribution of Fig. 7, and the velocity distribution was calculated for both. Both distributions are plotted in Fig. 7 and clearly show the sensitivity to small variations in  $M_m/M_p$  and  $r_m/r_p$ .

In general, agreement between the analytic and experimental results is considered satisfactory. The only significant departure is noted near the cylindrical wall in Figs. 6 and 7. This departure can be accounted for by considering viscous effects at the cylindrical wall, as has been done in Ref. 6.



To develop the expressions for  $r_c$  and  $Re_r$  in terms of the two known quantities, the normalized maximum tangential velocity  $v_m/v_p$  and the normalized radial location of the maximum tangential velocity  $r_m/r_p$ , Eq. (8) was differentiated once with respect to the radius  $r$ . The velocity gradient

$$\frac{d \frac{v}{v_p}}{d \frac{r}{r_p}}$$

was then set equal to zero and the resulting equation solved for radius  $r_m/r_p$  with the result

$$\frac{r_m}{r_p} = \frac{r_c}{r_p} \left[ \frac{(2 - Re_r) e^{Re_r/2} - 2}{Re_r (1 - Re_r)} \right]^{1/(2-Re_r)} \quad (9)$$

Equations (8) and (9) were then combined to obtain an expression for the maximum tangential velocity

$$\frac{v_m}{v_p} = (2 - Re_r) (1 - Re_r)^{(1-Re_r)/(Re_r-2)} \frac{\left(\frac{r_c}{r_p}\right)^{1-Re_r} [(2 - Re_r) e^{Re_r/2} - 2]^{(1-Re_r)/(2-Re_r)}}{\left(\frac{r_c}{r_p}\right)^{2-Re_r} [(2 - Re_r) e^{Re_r/2} - 2] + Re_r} \quad (10)$$

Equations (9) and (10) were solved simultaneously for  $Re_r$  and  $r_c/r_p$  in terms of  $r_m/r_p$  and  $v_m/v_p$ . The results are

$$\frac{r_c}{r_p} = \frac{r_m}{r_p} \left[ \frac{Re_r (1 - Re_r)}{(2 - Re_r) e^{Re_r/2} - 2} \right]^{1/(2-Re_r)} \quad (11)$$

and

$$\left(\frac{r_m}{r_p}\right)^{Re_r} + \left[ \frac{r_m}{r_p} \frac{v_p}{v_m} - \left(\frac{r_m}{r_p}\right)^2 \right] Re_r = \left[ 2 \frac{r_m}{r_p} \frac{v_p}{v_m} - \left(\frac{r_m}{r_p}\right)^2 \right] \quad (12)$$

Since Eq. (12) is transcendental, it must be solved by trial and error. The solution, obtained to any desired accuracy consistent with the accuracy of the experimentally determined  $r_m/r_p$  and  $v_m/v_p$ , is then used in Eq. (11) to obtain  $r_c/r_p$ . Equation (12) has two roots; the first is constant ( $Re_r = 2$ ) and hence is independent of  $r_m$  and  $v_m$ , while the second depends on  $r_m$  and  $v_m$  and is the one of interest here.

The maximum tangential velocity occurs at the core radius  $r_c$  ( $r_m = r_c$ ) when the radial Reynolds number equals 2.513; for smaller Reynolds numbers,  $r_m > r_c$ , as was determined from Eq. (9). Therefore, the results obtained from Eqs. (11) and (12) are meaningful only when the Reynolds number turns out to be less than 2.513. When the procedure just outlined is applied to Eq. (7), results valid for  $Re_e > 2.513$  are obtained. These are

$$\frac{r_m}{r_p} = \frac{r_c}{r_p} \left( \frac{2.513}{Re_r} \right)^{1/2} \quad (13)$$

$$\frac{v_m}{v_p} = 0.451 \frac{\left(\frac{r_c}{r_p}\right)^{1-Re_r} (2 - Re_r) e^{Re_r/2} Re_r^{1/2}}{\left(\frac{r_c}{r_p}\right)^{2-Re_r} [(2 - Re_r) e^{Re_r/2} - 2] + Re_r} \quad (14)$$

$$\frac{r_c}{r_p} = \frac{r_m}{r_p} \left( \frac{Re_r}{2.513} \right)^{1/2} \quad (15)$$

and

$$\frac{\left[ 2.513 \left( \frac{Re_r}{2.513} \right)^{Re_r/2} \left( \frac{r_m}{r_p} \right)^{Re_r-2} - 2 \right]}{(2 - Re_r) e^{Re_r/2}} = 0.715 \frac{v_p r_p}{v_m r_m} - 1 \quad (16)$$

The maximum Mach number  $M_m$  and its location  $r_m$  were determined for each experiment by applying Eq. (1) at several points in the vicinity of the maximum pressure gradient, plotting these  $M$  vs  $r$ , and selecting the maximum. Equation (1) was also applied at  $r_p$  to determine the peripheral Mach number  $M_p$ . This result is listed in Table 1. Equations (11) and (12) were then used to compute the core radius  $r_c/r_p$  and the radial Reynolds number  $Re_r$ , and these are also listed in Table 1. In addition, the various experiments are identified by the exit hole radius  $r_e$ , wall pressure  $p_w$ , and mass flow rate per unit length of vortex tube  $\dot{m}$ .

For several experiments, the Reynolds number turned out to be greater than 2.513; hence these values are invalid. This result was true of Run 47, which is the experiment shown in Figs. 5 and 8, and the Reynolds number and core radius were then recomputed from Eqs. (15) and (16). This second set of results is also listed in Table 1, where it is seen that the correct  $Re_r$  is approximately four times greater than that computed from Eq. (12). Also listed in Table 1 is the radial Reynolds number based on the mass flow rate and molecular viscosity

$\dot{m}/2\pi\mu_p$ . It is clearly seen that the value of the parameter  $Re_r$ , used in Eqs. (7) and (8), which best describes the flow field is considerably less than  $\dot{m}/2\pi\mu_p$ . This result is in general agreement with those of Refs. 11 and 12; however, it is not clear whether the reduced value of the effective Reynolds number is due to a reduced radial mass flow rate (because of the end wall boundary layers) or to an increased effective viscosity due to turbulence, or to both effects.

The core radius  $r_c$  is compared with the exit hole radius  $r_e$  in Table 1. For most experiments,  $r_c < r_e$ ; however, for Run 47,  $r_c > r_e$ . This means that under some conditions, the effective Reynolds number is a function of radius at radii greater than  $r_e$ . Also for Run 47,  $r_c/r_p > 1$ , which means that at least for that particular run the velocity distribution can best be described by a radius-dependent  $Re_r$  at all radii.

The maximum Mach number  $M_m$  is also plotted vs mass flow rate  $\dot{m}$  in Fig. 9, with exit hole radius  $r_e$  and wall pressure  $p_w$  as parameters. Points of constant exit hole radius and of constant wall pressure in Fig. 9 and

Table 1. Computed values of the effective radial Reynolds number and core radius

Run	$r_c/r_p$	$\dot{m}$ , lbm/sec-ft	$p_w$ , cm Hg (abs)	$T_c$ , °R	$M_p$	$Re_r$	$r_c/r_p$	$r_c/r_e$	$\dot{m}/2\pi\mu_p$
1	0.059	—	100.0	511	0.076	1.638	0.0143	0.242	—
2	↓	0.0109	199.8	510	0.082	—	—	—	—
3	↓	0.0164	300.4	512	0.071	—	—	—	—
4	↓	0.0219	400.1	505	0.046	—	—	—	—
5	↓	0.0274	499.8	503	0.046	2.229	0.0140	0.237	385
6	0.088	0.0060	100.1	512	0.077	1.696	0.0250	0.283	83
7	↓	0.0129	150.0	507	0.071	2.142	0.0219	0.248	181
8	↓	0.0189	200.0	503	0.089	2.079	0.0206	0.233	266

Table 1 (contd)

Run	$r_c/r_p$	$\dot{m}$ , lbm/sec-ft	$p_w$ , cm Hg (abs)	$T_o$ , °R	$M_p$	$Re_r$	$r_c/r_p$	$r_c/r_o$	$\dot{m}/2\pi\mu_p$
9		0.0288	300.1	499	0.127	1.691	0.0097	0.110	409
10		0.0383	400.0	497	0.109	2.046	0.0212	0.240	544
11		0.0477	500.0	498	0.120	1.950	0.0213	0.241	677
12	0.118	0.0080	100.2	513	0.104	—	—	—	112
13		0.0169	150.0	510	0.120	1.888	0.0224	0.190	236
14		0.0254	200.0	506	0.115	2.449	0.0454	0.385	356
15		0.0422	300.0	494	0.169	1.849	0.0236	0.176	597
16		0.0568	400.3	505	0.158	1.844	0.0187	0.158	799
17		0.0717	500.0	492	0.151	1.885	0.0207	0.175	1015
18	0.147	0.0104	100.2	510	0.104	2.045	0.0574	0.390	145
19		0.0229	150.1	507	0.127	2.356	0.0580	0.395	322
20		0.0348	200.0	497	0.148	2.682 <sup>a</sup>	0.0753	0.512	497
21		0.0568	300.5	493	0.195	2.052	0.0443	0.301	813
22		0.0712	370.5	496	0.207	2.132	0.0518	0.352	1017
23		0.0767	400.0	496	0.207	2.034	0.0440	0.299	1095
24		0.0964	500.0	501	0.200	2.018	0.0392	0.266	1380
25	0.177	0.0129	100.0	514	0.141	1.867	0.0575	0.325	179
26		0.0284	150.0	510	0.189	2.626 <sup>a</sup>	0.1175	0.661	397
27		0.0432	200.0	507	0.214	2.824 <sup>a</sup>	0.1318	0.746	610
28		0.0716	299.9	509	0.221	2.512	0.0800	0.452	1006
29		0.0916	400.0	501	0.261	2.281	0.0759	0.429	1293
30	0.236	0.0179	100.0	520	0.159	2.246	0.1269	0.538	246
31		0.0432	150.0	503	0.237	2.789 <sup>a</sup>	0.1784	0.754	615
32		0.0622	200.0	493	0.275	2.649 <sup>a</sup>	0.1590	0.674	900
33		0.0950	269.0	497	0.300	2.700 <sup>a</sup>	0.1500	0.636	1371
34		0.1003	270.0	501	0.316	2.095	0.0899	0.381	1495
35	0.294	0.0249	100.1	522	0.224	2.367	0.2568	0.874	343
36		0.0598	150.0	502	0.325	2.067	0.1780	0.605	854
37		0.0945	200.0	508	0.354	2.087	0.1434	0.486	1348
38	0.353	0.0333	100.0	512	0.261	4.821 <sup>a</sup>	0.5620	1.592	467
39		0.0786	150.0	490	0.327	5.145 <sup>a</sup>	0.4756	1.348	1147
40		0.1013	176.0	493	0.338	—	—	—	1473
41	0.412	0.0447	100.0	514	0.316	4.246 <sup>a</sup>	0.6001	1.456	629
42		0.0995	142.7	505	0.348	6.111 <sup>a</sup>	0.5164	1.252	1418
43	0.471	0.0577	100.0	511	0.316	21.660 <sup>a</sup>	0.9027	1.917	815
44		0.1000	124.5	507	0.393	6.927 <sup>a</sup>	0.6716	1.427	1417
45	0.530	0.0751	100.1	511	0.368	21.380 <sup>a</sup>	0.9832	1.855	1064
46		0.0990	111.2	510	0.431	6.028 <sup>a</sup>	0.7729	1.458	1419
47	0.589	0.0969	99.9	514	0.434	2.570 <sup>a</sup>	0.7078	1.202	1387
47		0.0969	99.9	514	0.434	10.603	1.397	2.373	1387

<sup>a</sup>These values of  $Re_r$  were obtained from Eq. (12) and, since they are greater than 2.513, are invalid.

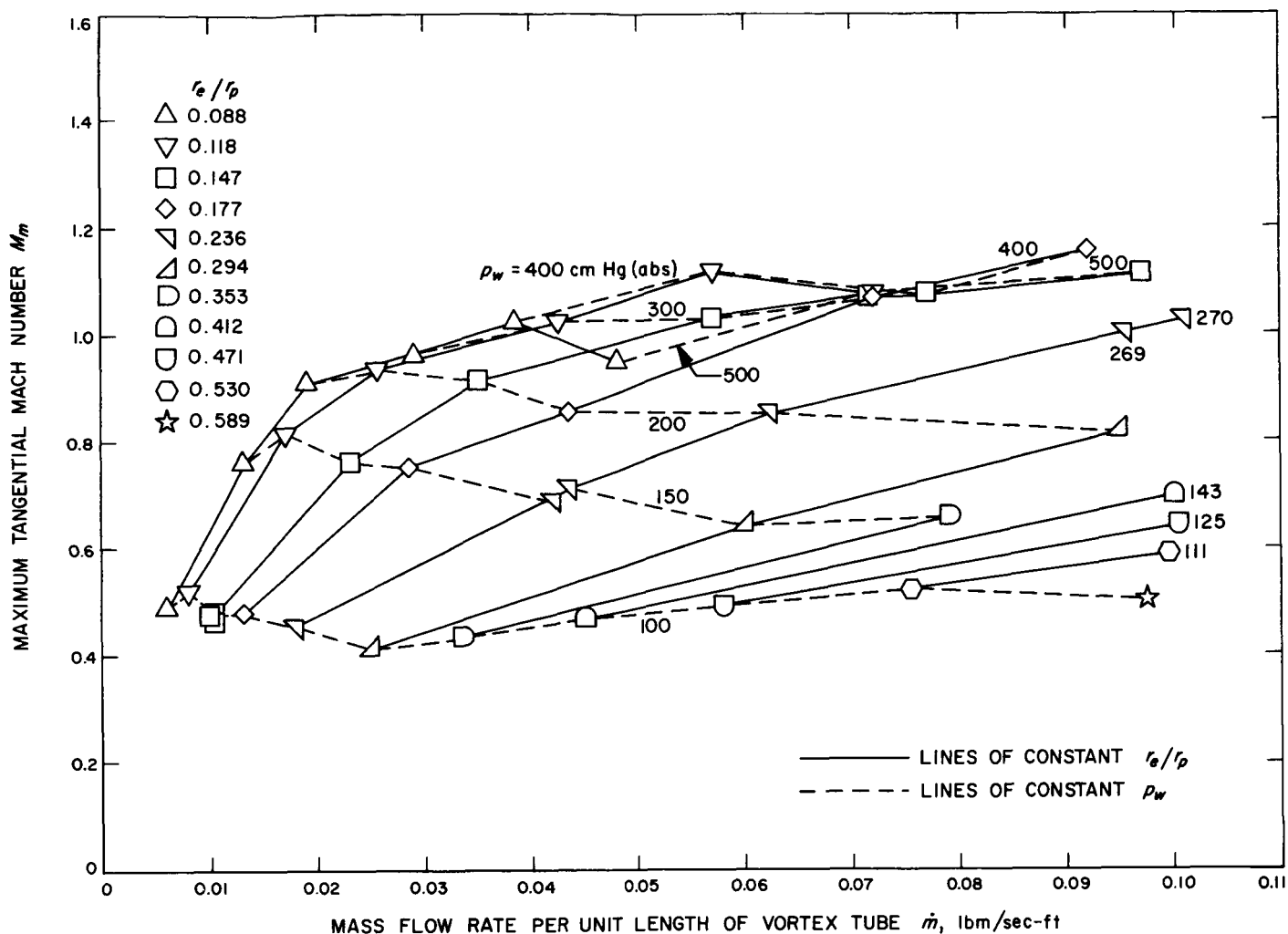


Fig. 9. Effect of exit hole diameter and mass flow rate on the maximum tangential Mach number

similar figures to follow are joined by straight lines to help clarify the trends; these straight lines are not intended as interpolations. Several experiments were performed at unique values of wall pressure, and the data points obtained are labeled with the pressure  $p_w$  in the figures. In a similar manner, the Mach number ratio  $M_m/M_p$  and the location of the maximum Mach number  $r_m/r_p$  are plotted in Figs. 10 and 11 respectively.

The tangential velocity at the periphery  $v_p$  was computed from the tangential Mach number  $M_p$  and measured manifold temperature  $T_o$  by assuming that the stagnation temperature at  $r_p$  was equal to  $T_o$ , hence

$$v_p = \left( \frac{\gamma R T_o M_p^2}{1 + \frac{\gamma - 1}{2} M_p^2} \right)^{1/2} \quad (17)$$

This velocity is plotted in Fig. 12 as a function of mass flow rate per unit length of vortex tube  $\dot{m}$ , with exit hole radius  $r_e$  and cylindrical wall static pressure  $p_w$  as parameters. In this figure, the points for which the driving jets were found to be subsonic are closed and those for the sonic jets are open.

The velocity of the fluid at the exit plane of the driving jet tube was computed from the measured manifold pressure and temperature, the measured cylindrical wall static pressure, and the total mass flow rate by assuming that the flow in the jet tubes followed the Fanno Line relationships of Ref. 13. Appropriate corrections, as described in Ref. 14, were made for losses incurred at the jet tube inlets. The resulting jet velocity  $v_{jet}$  is shown in Fig. 13 as a function of total mass flow rate per unit length and exit orifice diameter. It can be seen that for

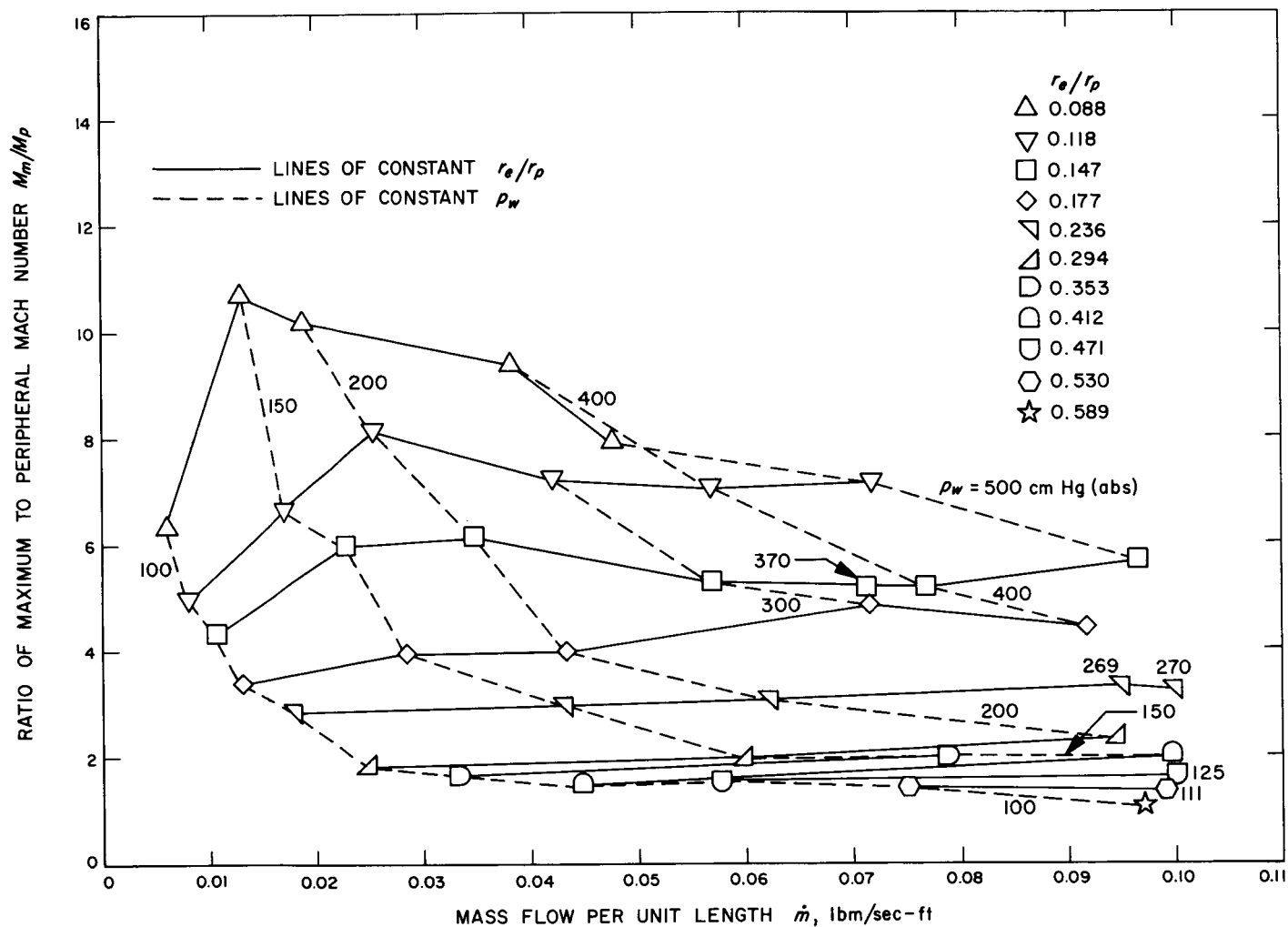


Fig. 10. Effect of exit hole diameter and mass flow rate on ratio of the maximum to the peripheral Mach number

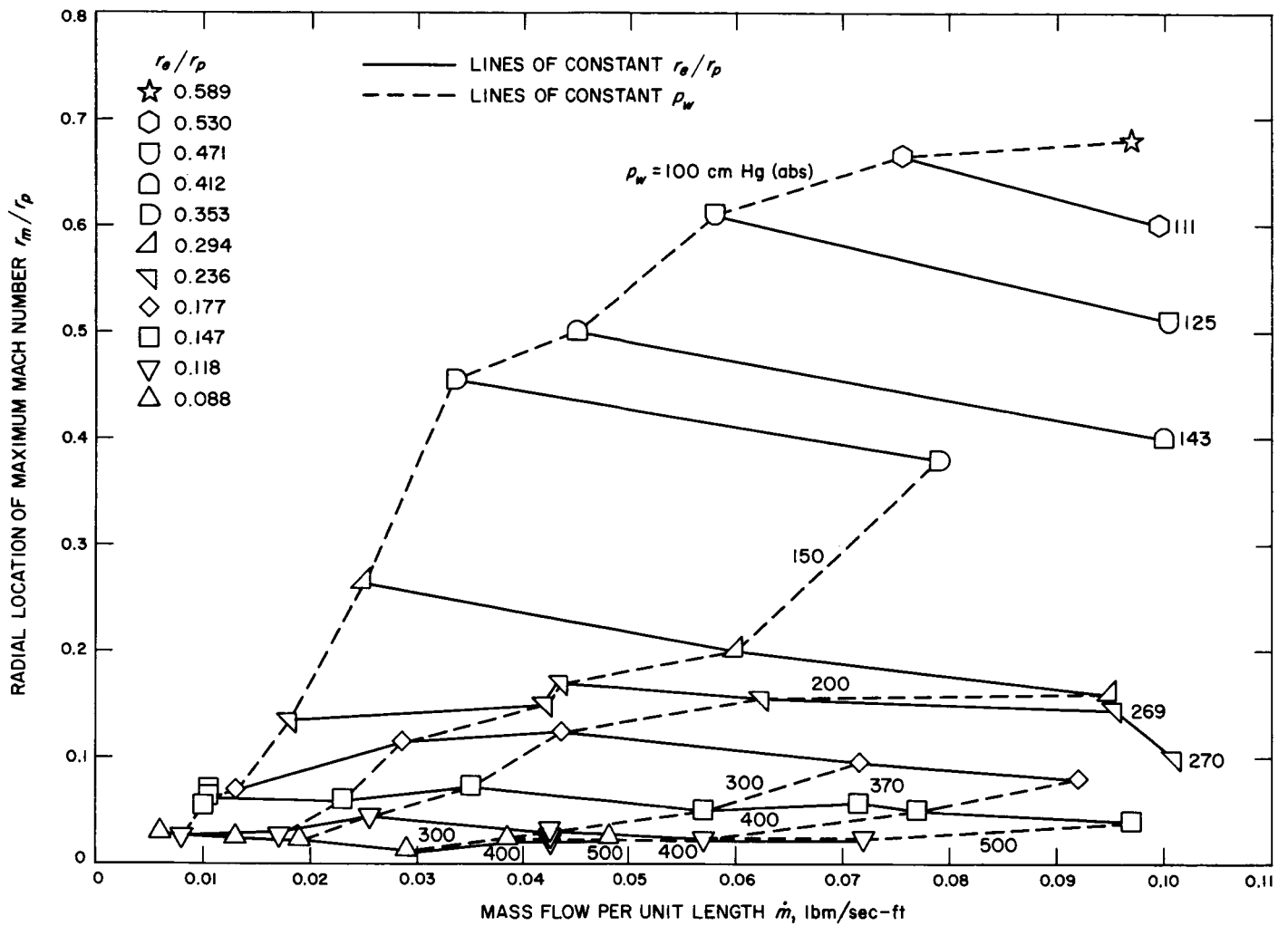


Fig. 11. Effect of exit hole diameter and mass flow rate on the radial location of the maximum tangential Mach number

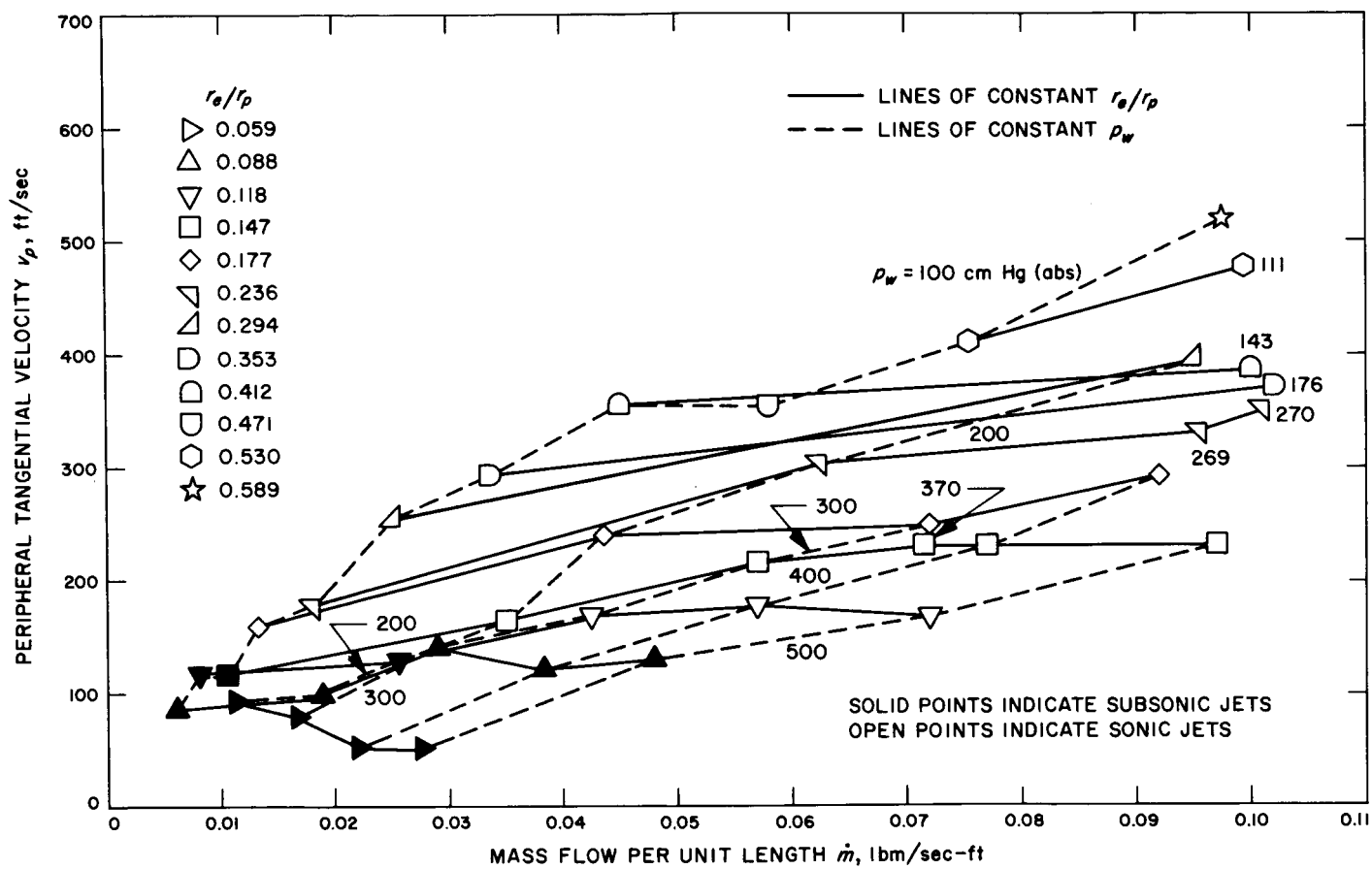


Fig. 12. Effect of exit hole diameter and mass flow rate on the peripheral tangential velocity

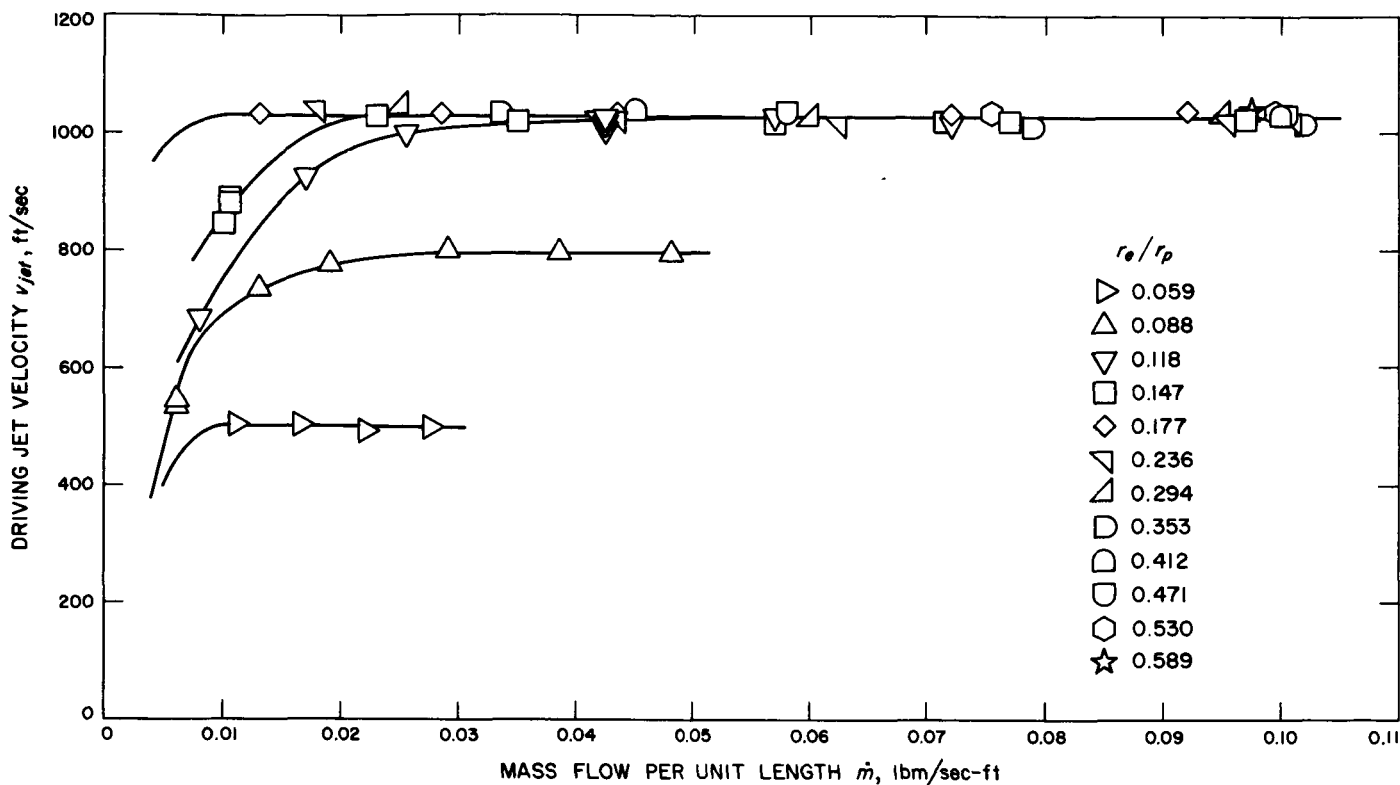


Fig. 13. Velocity of the driving jets at the jet tube exit plane

most of the experiments the jet exit velocity was sonic and therefore independent of the cylindrical wall static pressure and hence of the exit hole diameter. Sonic velocity corresponding to the computed temperature of the fluid at the exit plane of the driving jet tubes varied from 1006 to 1040 ft/sec. For exit hole to vortex tube diameter ratios of 0.056 and 0.083, the jet exit velocity does not approach the sonic condition as the mass flow rate is increased. Apparently, for these small exit holes, the increase in wall pressure  $p_w$  with increasing mass flow rate is sufficient to prevent the jet velocity from becoming sonic. This rapid increase of  $p_w$  with mass flow rate for the smaller exit holes is clearly seen in Fig. 14. However, the flow in the exit holes may have been sonic, since Fig. 15 shows the mass flow rate to be a linear function of the manifold pressure for all exit hole diameters, including the two smaller ones.

The average radial velocity of the fluid at the periphery of the vortex flow was computed for each experiment from the continuity equation:

$$u_p = \frac{R}{2\pi r_p} \frac{\dot{m}}{p_p} \frac{T_o}{1 + \frac{\gamma-1}{2} M_p^2} \quad (18)$$

The local values of the peripheral radial velocity would vary from this average value if there were axial velocities in the annulus between the periphery of the vortex flow  $r_p$  and the vortex tube wall  $r_w$ . However, it does not seem probable that appreciable axial velocities could be generated in so short a distance. There could also be local variations of the peripheral radial velocity because of the discrete inlet jets, but nothing can be said of their magnitude. The peripheral tangential velocity is shown as a function of the peripheral radial velocity in Fig. 16 with points of equal exit hole diameter designated by common symbols. It can be seen that within the scatter of the data the peripheral tangential velocity is correlated with the peripheral radial velocity throughout the range of mass flows and exit hole diameters investigated. Note also that the ratio of the tangential to radial peripheral velocities,  $v_p/u_p$ , is a constant, approximately equal to  $1.20 \times 10^3$ , for values of the peripheral tangential velocity between approximately zero and 350 ft/sec. It also appears that this ratio jumps to a second constant value of  $0.61 \times 10^3$  for  $v_p > 350$  ft/sec. In Ref. 15, it was shown that for any given vortex tube the ratio of tangential to radial Reynolds numbers is a function of the cylindrical wall skin friction coefficient only. Also, because of the way the Reynolds numbers are defined in



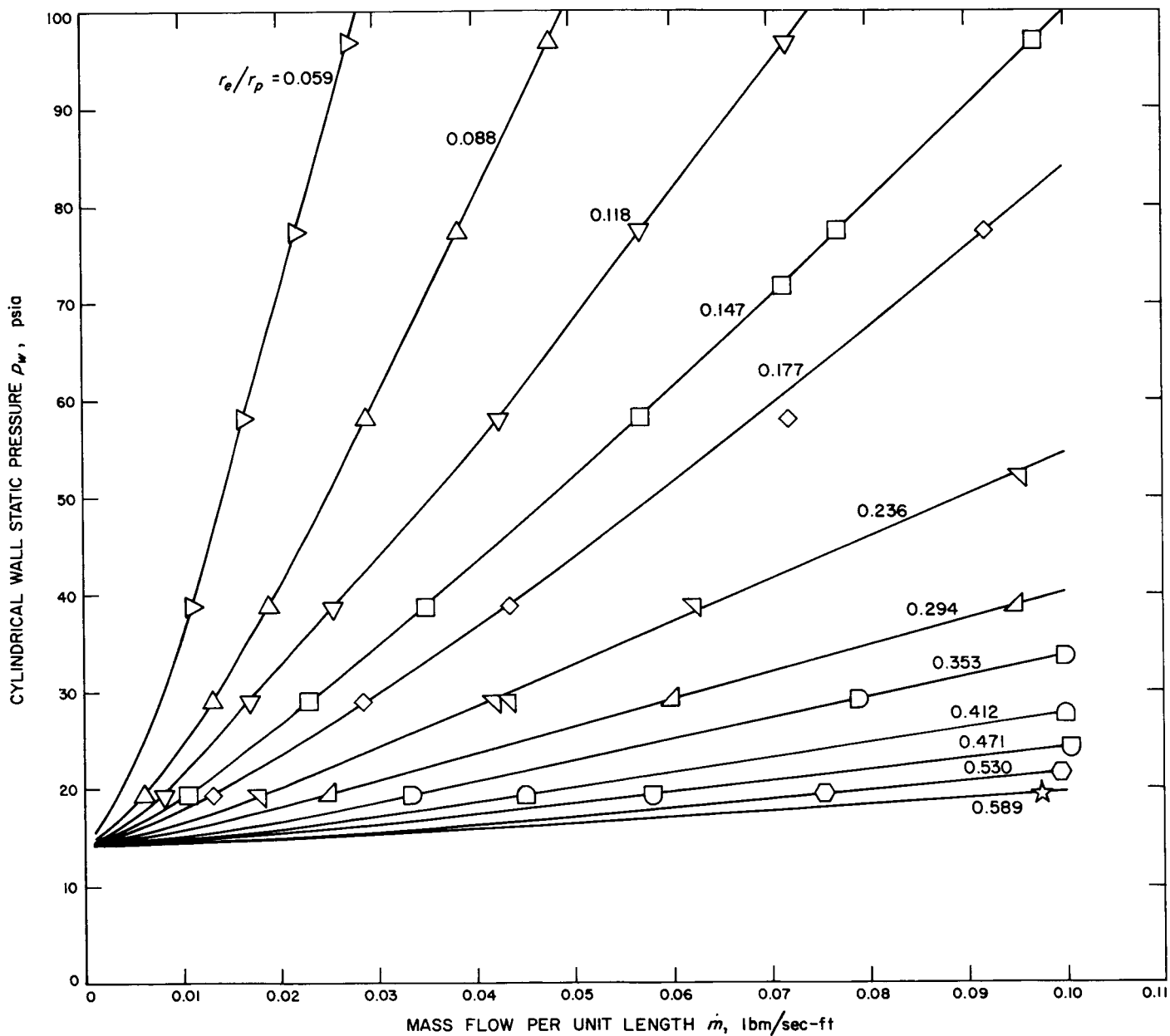


Fig. 14. Cylindrical wall static pressure

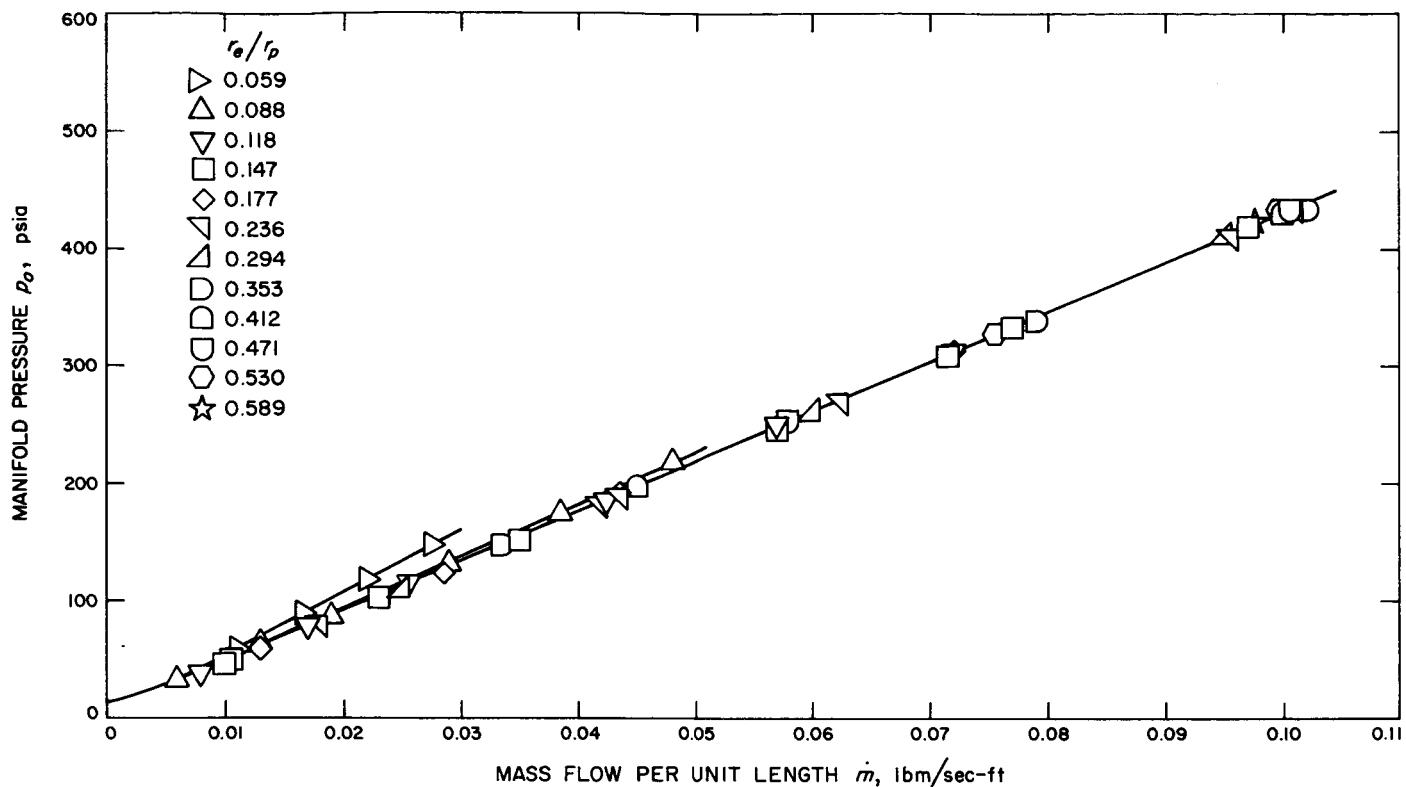


Fig. 15. Vortex tube manifold pressure

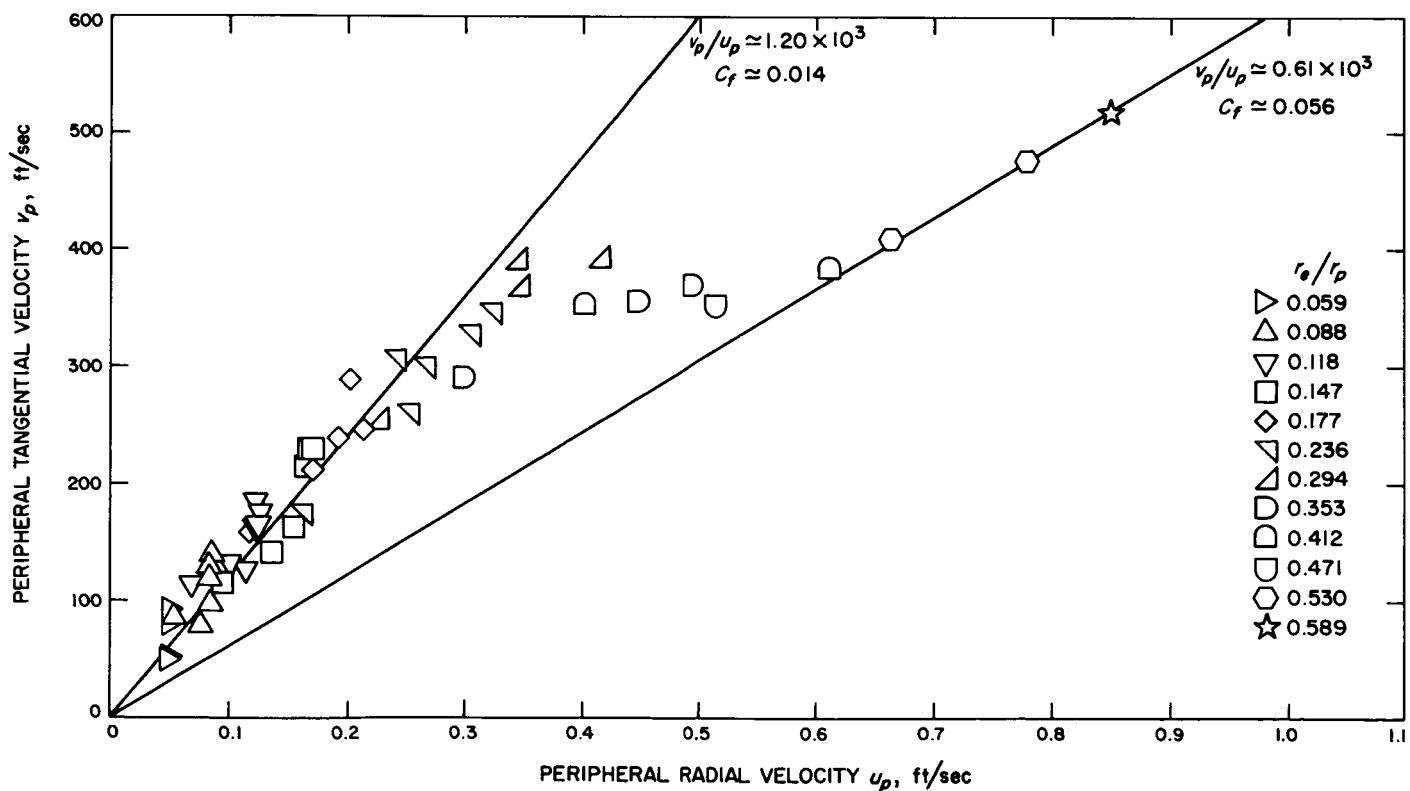


Fig. 16. Relationship between the peripheral tangential and radial velocities

Ref. 15, this ratio of Reynolds numbers is equivalent to the ratio of tangential to radial velocities. The expression for the Reynolds number ratio given in Ref. 15 can be inverted to obtain the following expression for the skin friction coefficient in terms of the Reynolds number or velocity ratio:

$$C_f = 2 \frac{\beta - \frac{v_p}{u_p}}{\left(\frac{v_p}{u_p}\right)^2} \quad (19)$$

The symbol  $\beta$  represents the ratio of vortex tube cylindrical wall area to the total driving jet exit area and, for the vortex tube used for this investigation,  $\beta = 1.10 \times 10^4$ . Through the use of Eq. (19), the skin friction was found to be 0.014 for  $v_p < 350$  ft/sec and 0.056 for  $v_p > 350$  ft/sec.

During this series of experiments, the exit hole diameter was used as a parameter. However, it is believed that the momentum loss at the periphery of the vortex flow is governed by the pressure or density level. Consequently, the data are presented accordingly. Of course the cylindrical wall pressure is itself governed by the exit hole diameter, and the relationship between the peripheral static pressure, total mass flow rate, and exit hole diameter is shown in Fig. 14 for completeness.

To complete the description of these several radial pressure distributions, the static pressures as measured at the center of the closed end wall are shown in Fig. 17. Points for which the exit hole radius was held constant are connected by solid lines, while those for which the cylindrical wall static pressure was constant are connected by dashed lines. It can be seen that for all the

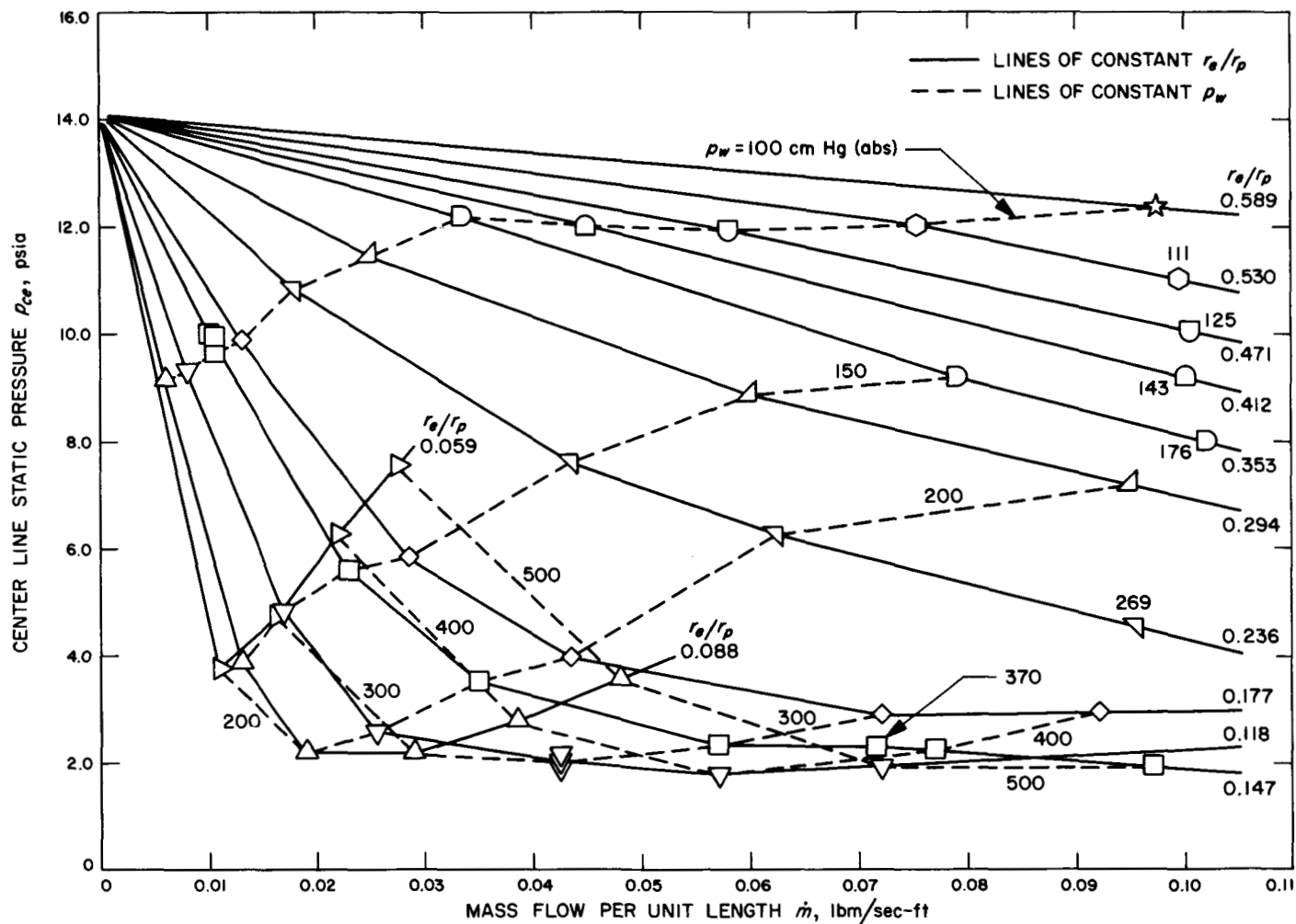


Fig. 17. Static pressure at center of closed end wall

conditions of these experiments the centerline static pressure was less than atmospheric. Since the vortex tube was open to the atmosphere at the exit hole, a recirculation must have been generated near the centerline at the exit end of the tube. However, measurements discussed in Ref. 16 indicate that this recirculation has very little influence on the internal flow structure. In general, for a given exit hole diameter, the centerline static pressure first decreases from one atmosphere, reaches a minimum, and then increases again as the total mass flow rate is increased. From the results obtained with the two smaller exit holes, it seems probable that the rise in centerline static pressure with increasing total mass flow rate is quite rapid and would produce pressures above ambient if the mass flow rates were high enough. It is interesting to note that there seems to be a lower limit of approximately 2 psia on this centerline static pressure, independent of exit hole diameter or  $p_w$ .

#### IV. Discussion

The radial static pressure distributions measured on the closed end wall of a simple vortex tube were found to be well behaved monotonic functions of radius for all mass flow rates and exit hole diameters investigated. It appears that for any given configuration the normalized pressure distributions rapidly approach a constant limiting distribution as the mass flow rate or reference pressure increases. This rapid convergence can be clearly seen in Fig. 3, for an exit hole diameter of 0.25 in., and in Fig. 4, where the exit hole diameter was 0.63 in. Once this limiting distribution is reached, the pressure gradient  $dp/dr$  becomes a linear function of the reference pressure  $p_p$  and hence of the pressure level in the vortex tube. This means that the term  $d \ln p/dr$ , which determines the tangential Mach number and is responsible for the binary diffusion in the gaseous-vortex-reactor concept of Ref. 1, is independent of  $p_p$  once this limit is reached. Since this reference pressure depends on the mass flow rate, as can be seen in Fig. 14 (the cylindrical wall static pressure  $p_w$  is approximately equal to  $p_p$ ), the driving potential for binary diffusion  $d \ln p/dr$  becomes independent of the mass flow rate as  $\dot{m}$  is increased. To sustain a dense annular cloud of fuel gas in the gaseous-vortex reactor with a minimum fuel loss rate, the term

$$\frac{1}{\dot{m}} \frac{d \ln p}{dr}$$

must be maximized; this was shown in Ref. 17. Therefore, a very definite limit exists on the propellant mass

flow rate capacity of a vortex tube, as used in the gaseous-vortex-reactor concept.

This result is generalized to other exit hole diameters in Fig. 10, where the maximum tangential Mach number  $M_m$ , which is approximately proportional to the maximum driving potential  $d \ln p/dr$ , is shown as a function of mass flow rate with exit hole diameter and cylindrical wall static pressure as parameters. The maximum  $M_m$ , if one exists, was not reached for the larger exit holes because of the mass flow limitations on the experimental equipment. It appears that, at least for the smaller exit holes, the maximum  $M_m$  achieved increases slightly with increasing exit hole diameter and that it requires more mass flow to achieve the maximum  $M_m$  as the exit hole diameter increases. Therefore, to optimize the vortex tube as a heavy gas separation device, one might consider making the exit hole diameter small. Of course the exit hole diameter is only one of several variables that must be considered before the heavy gas separation can be optimized. For example, the effect of mass flow rate and pressure level on the nature of the flow (laminar or turbulent) and on the end wall boundary layers, which have a profound effect on the vortex flow field, must be considered. To illustrate this point, note in Fig. 9 that for an exit hole radius ratio  $r_e/r_p$  of 0.147, the term  $M_m/\dot{m}$  decreases from approximately 50 at low  $\dot{m}$  to 10 at high mass flow, whereas the separation measurements of Ref. 17, made with the same vortex tube and exit hole diameter, show an increase of heavy gas separation as  $\dot{m}$  increases.

The peripheral tangential velocity  $v_p$  is plotted as a function of mass flow rate  $\dot{m}$  with cylindrical wall static pressure and exit hole diameter as parameters in Fig. 12 and as a function of peripheral radial velocity  $u_p$  with exit hole diameter as a parameter in Fig. 16. The significant trend in Fig. 12 is the decrease of the peripheral tangential velocity with increasing pressure and decreasing exit orifice size. This means that for a given total mass flow rate the angular momentum available to the vortex flow field at its periphery,  $\dot{m}v_p r_p$ , decreases with increasing pressure. Unless some way is found to substantially overcome this loss, the peripheral tangential velocity will be small indeed for the 170- to 500-atmosphere cylindrical wall pressure assumed in Ref. 1 for a practical gaseous-vortex reactor. Increasing the peripheral tangential velocity by large increases in the total mass flow rate would not be feasible unless the excess mass flow is bled off, for example by wall suction, before it enters the region where the maximum diffusion rates are expected

to occur. The idea of wall suction was analytically investigated in Ref. 18 and experimentally investigated in Ref. 11. In this respect, the ability of the end wall boundary layers to bypass a very large fraction of the injected mass flow around the regions where diffusion and the consequent high fuel concentrations are to occur might be an advantage.

A further significant effect found in these results is the apparent jump in cylindrical wall skin friction seen in Fig. 16. Apparently the flow along the cylindrical wall changes character at a tangential velocity of approximately 350 ft/sec, somewhat like the transition from laminar to turbulent flow in pipes. This effect would further reduce the angular momentum available to the vortex flow field.

The angular momentum available to the vortex flow field is given approximately by  $\dot{m}v_p r_p l$  and the angular momentum injected into the vortex tube by approximately  $[\dot{m}v_{jet}l + (p_{jet} - p_p)A_{jet}]r_p$ . If the contribution to the injected momentum represented by the pressure difference  $(p_{jet} - p_p)$  is neglected, the ratio of average peripheral to injected angular momentum is approximately  $v_p/v_{jet}$ . From Figs. 12 and 13, this ratio is seen to vary from approximately 0.1 to 0.5. This means that from 50 to 90% or more of the injected momentum is dissipated by viscous effects in the vicinity of the cylindrical wall of the vortex tube. Therefore, to improve the performance of vortex tubes, for whatever purpose, consideration must first be given to these losses at the cylindrical wall. One method of overcoming these losses (wall suction) has been referred to (Refs. 11 and 18). A second interesting method has been proposed and investigated by the authors of Ref. 19. This method consists essentially of a number of vortex flows rolling on each other like rollers in a printing press. In principle, this flow would eliminate velocity gradients over part of the boundaries, thereby reducing the total momentum loss.

The complete results of Figs. 9 and 11 show that for any given total mass flow rate, as the exit hole diameter decreases, the maximum Mach number increases and occurs at smaller radii. This seems to indicate that as the

exit hole becomes smaller for a given mass flow rate, the fluid and hence angular momentum is being convected to smaller radii. At the same time, Fig. 12 shows that the peripheral tangential velocity decreases as the exit hole becomes smaller, again for a given mass flow rate. Therefore, the total effect of decreasing the exit hole diameter is to decrease the angular momentum available to the vortex flow at its periphery and to force this angular momentum to be convected to regions of smaller radii. Note also that for exit hole diameter ratios equal to or less than 0.294, the maximum tangential Mach number is found to occur at a radius less than the exit hole radius; for diameter ratios equal to or greater than 0.353, the maximum tangential Mach number is found at radii greater than the exit hole radius.

## V. Conclusions

The radial static pressure distribution has been measured on the closed end wall of a right circular cylinder vortex tube for a range of exit hole diameters and mass flow rates. From these measurements it is concluded that

- (1) A limiting radial distribution of tangential Mach number and binary diffusion driving potential  $d \ln p/dr$  exists for any given configuration. As the mass flow rate increases, this limit is soon reached, and further increases of  $\dot{m}$  have no effect on  $p/p_p$ , on  $M$ , or on  $d \ln p/dr$ .
- (2) To improve the performance of a vortex tube (extending the limits on  $M$  or on  $d \ln p/dr$ ), a fruitful area to concentrate on would be the loss mechanism at the cylindrical wall.

Several experimentally determined radial distributions of tangential Mach number have been compared with the radial distribution of tangential velocity computed from a particular form of the tangential momentum equation. It is concluded that this method of computing  $v = f(r)$  gives reasonably accurate results. However, the computation requires values for two parameters,  $Re_r$  and  $r_c/r_p$ , and there appears to be no easy way of selecting the values that correspond with any particular set of experimental conditions.

## Nomenclature

$a$	distance from disk centerline to pressure tap, 1.063 in.	$\gamma$	ratio of specific heats
$A$	cross-sectional area	$\Gamma$	circulation, defined as $\nu r$
$C$	a positive constant of arbitrary value	$\theta$	angular orientation of disk, measured from vortex tube centerline
$C_f$	average skin friction coefficient	$\mu$	molecular viscosity
$l$	length of vortex tube	$\nu$	kinematic viscosity
$\dot{m}$	mass flow per unit length of vortex tube	$\phi$	angular orientation of selsyn armature
$M$	tangential Mach number		
$n$	exponent in approximate equation for tangential velocity		
$p$	static pressure		
$r$	radial coordinate		
$R$	gas constant		
$Re_r$	radial Reynolds number, defined as $(-ur/\nu)$		
$T$	static temperature		
$u$	radial velocity		
$v$	tangential velocity		
$w$	axial velocity		
$z$	axial coordinate		
$\beta$	ratio of vortex tube cylindrical wall area to total driving jet exit area		

### Subscripts

$c$	refers to radius of core in analytic model
$ce$	value at centerline of vortex tube
$e$	value at edge of exhaust hole
$jet$	refers to driving jets
$m$	refers to maximum tangential Mach number
$o$	value in vortex tube manifold
$p$	value at reference radius, equal to 2.12 in.
$w$	value at cylindrical wall of vortex tube

## References

1. Kerrebrock, J. L., and Meghreblian, R. V., *An Analysis of Vortex Tubes for Combined Gas-Phase Fission-Heating and Separation of the Fissionable Material*, ORNL CF-57-11-3 Rev. 1, Oak Ridge National Laboratory, Oak Ridge, Tenn., April 11, 1958. See also Kerrebrock, J. L., and Meghreblian, R. V., "Vortex Containment for the Gaseous-Fission Rocket," *Journal of Aerospace Sciences*, Vol. 28, No. 9, September 1961, pp. 710-724.
2. Massier, P. F., "Axisymmetric Steady Flow of a Swirling Compressible Fluid Through a Convergent-Divergent Nozzle Without External Heat Transfer," *Space Programs Summary No. 37-33, Vol. IV*, Jet Propulsion Laboratory, Pasadena, Calif., June 30, 1965, pp. 133-141.
3. Pai, S.-I., *Viscous Flow Theory I—Laminar Flow*, D. Van Nostrand Company, Inc., Princeton, N. J., 1956.
4. Einstein, H. A., and Li, H., "Steady Vortex Flow in a Real Fluid," *1951 Heat Transfer and Fluid Mechanics Institute, Preprints of Papers*, Stanford University Press, Stanford, Calif., June 1951, pp. 33-43.

## References (contd)

5. Pengelley, C. D., "Flow in a Viscous Vortex," *Journal of Applied Physics*, Vol. 28, No. 2, January 1957, pp. 86-92.
6. Rietema, K., and Krajenbrink, H. J., "Theoretical Derivation of Tangential Velocity Profiles in a Flat Vortex Chamber—Influence of Turbulence and Wall Friction," *Applied Scientific Research, Section A*, Vol. 8, 1959, pp. 177-197.
7. Lewellen, W. S., "A Solution for Three-dimensional Vortex Flows With Strong Circulation," *Journal of Fluid Mechanics*, Vol. 14, 1962, pp. 420-432.
8. Rosenzweig, M. L., Lewellen, W. S., and Ross, D. H., "Confined Vortex Flows With Boundary-Layer Interaction," *AIAA Journal*, Vol. 2, No. 12, December 1964, pp. 2127-2134.
9. Kerrebrock, J. L., and Keyes, J. J., Jr., *A Preliminary Experimental Study of Vortex Tubes for Gas-Phase Fission Heating*, ORNL-2660, C-86-Nuclear Rocket and Ram-Jet Engines, Oak Ridge National Laboratory, Oak Ridge, Tenn., February 1959.
10. Roschke, E. J., "An Examination of Vortex Strength in a Compressible Viscous Vortex," *Space Programs Summary No. 37-20, Vol. IV*, Jet Propulsion Laboratory, Pasadena, Calif., April 30, 1963, pp. 73-76.
11. Keyes, J. J., Jr., and Dial, R. E., *An Experimental Study of Vortex Flow for Application to Gas-Phase Fission Heating*, ORNL-2837, C-86-Nuclear Rocket and Ram Jet Engines, Oak Ridge National Laboratory, Oak Ridge, Tenn., June 13, 1960.
12. Ross, D. H., *An Experimental Investigation of Turbulent Shear in Jet-Driven Vortex Chambers*, Report No. ATN-64(9227)-5, Aerospace Corporation, El Segundo, Calif., October 1, 1964.
13. Keenan, J. H., and Kaye, J., *Gas Tables*, John Wiley and Sons, Inc., New York, N. Y., 1948.
14. *Chemical Engineers Handbook*, Third Edition, John H. Perry, Editor, McGraw-Hill Book Company, Inc., New York, N. Y., 1950.
15. Roschke, E. J., "Some Gross Effects of Cylindrical Wall-Friction and End-Wall Boundary-Layer Flow on Confined Vortex Flows," *Space Programs Summary No. 37-21, Vol. IV*, Jet Propulsion Laboratory, Pasadena, Calif., June 30, 1963, pp. 102-108.
16. Kendall, J. M., Jr., *Experimental Study of Compressible Viscous Vortex*, Technical Report No. 32-290, Jet Propulsion Laboratory, Pasadena, Calif., June 1962.
17. Pivrotto, T. J., *An Experimental and Analytical Investigation of Concentration Ratio Distributions in a Binary Compressible Vortex Flow*, Technical Report No. 32-808, Jet Propulsion Laboratory, Pasadena, Calif., March 15, 1966.
18. Kerrebrock, J. L., and Lafyatis, P. G., *Analytical Study of Some Aspects of Vortex Tubes for Gas-Phase Fission Heating*, ORNL-CF 58-7-4, Oak Ridge National Laboratory, Oak Ridge, Tenn., July 21, 1958.

### References (contd)

19. Rosenzweig, M. L., Lewellen, W. S., and Kerrebrock, J. L., *The Feasibility of Turbulent Vortex Containment in the Gaseous Fission Rocket*, American Rocket Society Preprint 1516A-60, presented at the Annual ARS Meeting, Washington, D. C., December 5-8, 1960.